Physics Reports 469 (2008) 59–92

Contents lists available at ScienceDirect

Physics Reports

journal homepage: www.elsevier.com/locate/physrep

Dynamics of coin tossing is predictable

J. Strzałko, J. Grabski, A. Stefański, P. Perlikowski, T. Kapitaniak *

Division of Dynamics, Technical University of Łódź, Stefanowskiego 1/15, 90-924 Łódź, Poland

ARTICLE INFO

Article history:
Accepted 14 August 2008
Available online 7 September 2008
editor: I. Procaccia

PACS:
45.40.-f
05.45.-a

Keywords:
Coin tossing
Coin modeling
Predictability
Basins of attraction
Quaternions

ABSTRACT

The dynamics of the tossed coin can be described by deterministic equations of motion, but on the other hand it is commonly taken for granted that the toss of a coin is random. A realistic mechanical model of coin tossing is constructed to examine whether the initial states leading to heads or tails are distributed uniformly in phase space. We give arguments supporting the statement that the outcome of the coin tossing is fully determined by the initial conditions, i.e. no dynamical uncertainties due to the exponential divergence of initial conditions or fractal basin boundaries occur. We point out that although heads and tails boundaries in the initial condition space are smooth, the distance of a typical initial condition from a basin boundary is so small that practically any uncertainty in initial conditions can lead to the uncertainty of the results of tossing.

Contents

* Corresponding author.
E-mail address: tomaszka@p.lodz.pl (T. Kapitaniak).

0370-1573/$ – see front matter © 2008 Elsevier B.V. All rights reserved.
doi:10.1016/j.physrep.2008.08.003

Nomenclature

e_0, e_1, e_2, e_3 Euler parameters (normalized quaternions),
$\mathbf{r}$, $\mathbf{r}_A$, $\mathbf{r}_B$, $\mathbf{r}_C$ coin point position vectors,
$\mathbf{R}_{\varphi_i}$ rotation matrices for the rotation through angle φ_i,
$\mathbf{R}_{i/j}$ coordinate transformation matrices from xyz coordinate frame to $\xi\eta\zeta$ coordinate frame,
r, h dimensions (radius and thickness) of coin, m,
ψ, ϑ, φ rotation angles of coin (Euler angles), rad,
ω_ξ, ω_η, ω_ζ coin angular velocity components in body frame $\xi\eta\zeta$, rad/s,
φ_1, φ_2, φ_3 angles of rotation, rad,
$\mathbf{J}_B$ inertia matrix of the coin (mass moments of inertia of the coin with respect to $B\xi\eta\zeta$ frame),
$\mathbf{J}_C$ inertia matrix of the coin (mass moments of inertia of the coin with respect to $C\xi\eta\zeta$ frame),
J_ξ, J_η, J_ζ coin mass moments of inertia for $B\xi\eta\zeta$ (or $C\xi\eta\zeta$) axes, kg m^2,
$J_{\xi\eta}$, $J_{\eta\zeta}$, $J_{\zeta\xi}$ inertia products of the coin in $B\xi\eta\zeta$ (or $C\xi\eta\zeta$) frame, kg m^2,
λ_n, λ_τ dimensional air resistance coefficients — in normal and tangent directions,
χ restitution coefficient,
S_x, S_y, S_z components of reaction force impulses, N s,
$\mathbf{M}$ mass matrix of the coin ($\mathbf{M} = \mathrm{diag}\,[m\ \ m\ \ m]$),
m mass of the coin, kg,
$\mathbf{f}_1, \ldots, \mathbf{f}_3$ vectors of air resistance force components,
$\mathbf{m}_1$, $\mathbf{m}_2$, $\mathbf{m}_3$ vectors of air resistance moment components,
M_ξ, M_η, M_ζ air resistance moment components,
E, T, V total mechanical energy, kinetic and potential energy of the coin, kg m^2/s^2,
t time, s,
$\mathbf{v}_{A_i}$ vector of velocity of coin point A_i,
xyz base reference frame (fixed),
$x'y'z'$ body (coin) embedded frame (parallel to the spatial frame xyz),
$\xi\eta\zeta$ body (coin) embedded frame,
ξ_A, η_A, ζ_A, ξ_C, η_C, ζ_C point A (C) position vector components in body embedded frame,
x, y, z displacements of the coin mass center in the xyz frame, m,
$\dot{x}', \ldots, v'_{Az}$ components of body point velocity vectors after body collision, m/s,
$\boldsymbol{\omega}_\xi$ vector of angular velocity of the coin in body embedded frame $\xi\eta\zeta$,
$\boldsymbol{\omega}$ vector of the coin angular velocity components in base reference frame xyx,
$\boldsymbol{\Omega}_\xi$ skew (antisymmetric) matrix of $\xi\eta\zeta$ coin angular velocity components.

1. Introduction

The historical origin of coin tossing is the interpretation of a chance outcome as the expression of divine will. A well-known example of such a selection (although not explicitly involving a coin) is the episode from *The Holy Bible* [1] in which the prophet Jonah was chosen by lot to be cast out of the boat, only to be swallowed by a giant fish (Book of Jonah, Chapter 1). The coin tossing as a game was known to the Romans as 'navia aut caput' ('ship or head'), as some coins had a 'ship' on one side and the head of the Roman emperor on the other. In medieval England, this game was referred to as 'cross and pile' and was usually played using homemade coins with a cross on one side.

The coin tossing is a simple and fair way of deciding between two arbitrary options. It is assumed that it provides even odds to both sides involved, requiring little effort and preventing the dispute from escalating into a struggle. It is used widely in sport and to decide about arbitrary factors such as; which side of the field a team will start the game from, or which side will attack or defend initially. In team sports (soccer, American football, ice hockey, etc.) it is often the team captain who makes the call, while the referee usually tosses a coin. A spectacular case took place in the 1968 European Football (Soccer) Championship. The semi-final game between Italy and the Soviet Union finished 0–0 after an extra-time. At that time penalty shoot-out was not introduced and the decision was reached to toss a coin to see who gets to the final, rather than play a replay. Italy won, and went on to become the European champion.

In some jurisdictions, a coin is tossed to decide between two candidates who poll an equal number of votes in an election, or two companies tendering the equal prices for a project (such a situation occurred in Toronto in 2003). In more casual settings, a coin tossing is used simply to resolve the arguments between friends or family members.

It is commonly taken for granted that the toss of a coin is *random*. This statement is fundamental in the probability theory [17,39,32] and usually two types of coins are mathematically distinguished. The coin is *fair* if the probability of heads and tails is equal, i.e., Prob(heads) = Prob(tails) = 1/2. The coin has the known *bias* $\theta \in (0, 1]$ if Prob(head) $= 1/2(1+\theta)$. Tossing the coin is frequently used to describe the problems concerning random walks on scenery [24,8,28]. The random

walk is an example of a stochastic process going on in time; namely, the motion of a particle which is randomly hoping backward or forward [22]. Backward or forward steps can be determined by tossing a coin.

One of the random walk problems is a variation of Gambler ruin game [60,40,31,15,23] in which a rich player gambles with a set amount of money while the poor one starts out with zero capital, and is allowed to toss a coin in order to try to win the money. If the coin is heads, the poor player wins a dollar but if it is tails, the player loses a dollar. The poor player is always allowed to win the first toss, and is allowed to toss n times, even when the amount of money lost reaches zero. The studies of Cooper [10,11] show that the dynamics in this process is chaotic as the result of the fluctuations in the variance of the amount of money [10], and can model the on–off intermittency [58]. Coin tossing can be also considered as a billiard problem [5].

The toss of the coin belongs to the group of classical randomization mechanical systems. Other elements in this group are e.g. roulette and Buffon's needle. The analysis of the dynamical behavior of roulette goes back to Poincare [59]. His results suggest that as the roulette ball is spun more and more vigorously the outcome number is independent of the initial conditions (initial conditions are washed out). For a large number of trials the numbers become close to the uniform distribution. Later studies [6,7] suggest that the real roulette may not be vigorous enough to wash out initial conditions. E. Hopf studies of Buffon's needle [25–27] show independence of the successive outcomes but also give examples where the initial conditions are not washed out. More details on these studies can be found in [43,57,64,16].

The physical definition of the fair coin is completely lacking. One cannot expect the detailed characteristic to be general for every coin as many sizes and shapes of real coins exist. We consider that the coin is a rigid body with the round shape and assume that the physical equivalence of the fair coin is an *ideal coin* with uniform mass distribution and the equivalence of the coin with bias is an *imperfect coin* with nonuniform mass distribution. In both cases the coin has *no intrinsic randomness* and what is relevant is the relation of the initial position (initial conditions) of the coin to the precision of the coin tosser.

One can assume that the equations of motion are Newton's equations, with no external source of random influence, i.e., the fluctuations of air, thermodynamic or quantum fluctuations of the coin, the coin tosser and the surface on which it falls are negligible. Under these assumptions it is possible to construct a mapping of the initial conditions to a final observed configuration. The initial conditions are position, configuration, momentum, and angular momentum at the beginning of the motion. There are three possible final configurations: the coin terminates flat on the surface with its heads side up, its tails side up, or the coin balances on its edge. The first two configurations are stable (using the definitions of [67,9] one can call them stable point attractors). All initial conditions are mapped into one of the final configurations. The initial conditions which are mapped onto heads configuration create *heads basin of attraction* while the initial conditions mapped onto tails configuration create *tails basin of attraction*. The boundary which separates heads and tails basins consists of initial conditions mapped onto the coin standing on the edge configuration. For an infinitely thin coin this set is a set of zero measure and thus with probability one the coin ends up either heads or tails. For the finite thinness of the coin this measure is not zero but the probability of edge configuration to be stable is low. In the paper [52] it is shown that an American 25 cents (nickel) coin lands on the edge about one time in 6000 tosses. The problem of how a coin must be tossed to have probability 1/3 of landing on the edge is discussed in [51].

As one can observe there is nothing nondeterministic in the described mapping, so the toss of the physical coin has to be obviously nonrandom. From the point of view of the dynamical systems the outcome of the tossing coin should be deterministic. As the initial conditions — final configuration mapping is strongly nonlinear one can expect deterministic unpredictability due to the sensitive dependence on the initial conditions or fractal basin boundaries. In other words one can pose the question, *is anything chaotic in the dynamics of the tossed coin which can produce a random like behavior* [19,56,5].

The detailed studies of the tossed coin dynamics started with the work of Keller [38]. His results can be summarized in the following way. Consider an ideal coin and assume that the center of the mass which can move vertically is at the height $z(t)$ at time t. In addition to its vertical motion, the coin is assumed to be rotating about a horizontal axis that lies along the diameter of the coin. Let x be the axis which is parallel to this rotation axis. One can describe the angular position of the coin at time t by the angle $\vartheta(t)$ between the positive z axis and the normal to the side of the coin which is up at $t = 0$ (see Fig. 1). When $\vartheta(0) = 0$ the coin rotates with n_0 revolutions per second (angular velocity $\omega_0 = 2\pi n_0$).

If the initial velocity in the up direction z is v_0, after t seconds, a coin tossed at the initial height z_0 will be at the height $z_0 + v_0 t - (g/2)t^2$, where g is the acceleration due to the gravity. If the coin is caught when it returns to the initial height z_0, the elapsed time t^* of the coin motion satisfies $t^* = 2v_0/g$, so the coin has revolved $n = 2n_0 v_0/g$ times. If n is between $2j$ and $2j+1$, where $j = 0, 1, 2, \ldots$ the initial side will be up-most and if $n \in (2j+1, 2j+2)$ the opposite side will be up-most. Fig. 2 shows the decomposition of the phase space $(\omega_0/\pi, v_0/g)$ into regions where the coin comes up as it started (black regions) or opposite (white regions). These two regions are separated by the hyperbola $2n_0 v_0/g = j$ (or $\frac{\omega_0}{\pi}\frac{v_0}{g} = j$).

The coin bouncing on the landing surface has been analyzed by Vulović and Prange [67]. They assume an explicit model of inelastic collisions that determines the coin's eventual resting place. In the numerical studies they show that the decomposition of the phase space $(\omega/\pi, v_z/g)$ is remarkably similar to one shown in Fig. 2 but in the regions far from zero the regions which determine the final side of the coin are narrower. More details about these studies will be given in Section 5.2. In the study of Zeng-Yuan and Bin [71] both bouncing and air resistance have been considered but spin and precession are not taken into account so that the obtained results are valid only for two degrees of freedom ideal coin. Finally one should mention the work of Diaconis, Holmes and Montgomery [13] where the motion of the coin is considered in 3D space. Their theoretical and experimental studies allow stating that the probability that the coin will rest on the side which is up at the initial moment is larger than the probability of the other side and equal to 0.51.

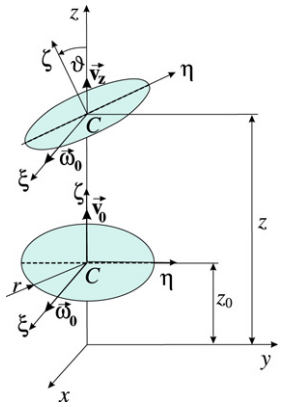

Fig. 1. Keller's [38] coin tossing model (rotation around axis (ξ) parallel to x).

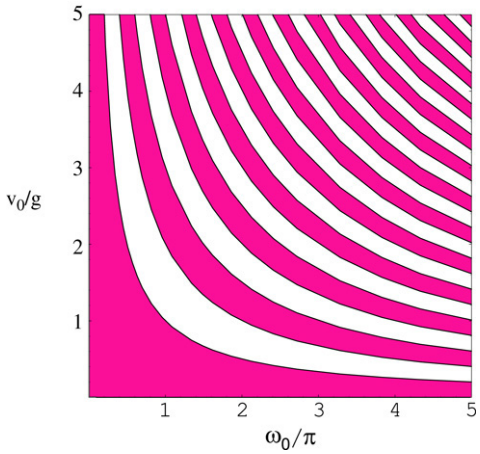

Fig. 2. Decomposition of the phase space (ω_0/π, v_0/g) into regions where the coin comes up as it started (white regions) or opposite (dark regions) [38].

Our studies give arguments supporting the statement that the outcome of the coin tossing procedure is fully determined by the initial conditions, i.e., no dynamical uncertainties due to the exponential divergence of initial conditions or fractal basin boundaries have been identified. We analyze the dynamics of general 3D model of a coin. The cases of uniform and nonuniform coins as well as the influence of air resistance and the impacts between the coin and surface are considered.

This paper is organized as follows. Section 2 presents the results of experimental observations of the tossed coin motion. In Section 3 the coin, a round disk with nonuniform mass distribution is described as a rigid body. It is assumed that the coin is released above a plain floor. Euler angles and Euler parameters (normalized quaternions) are used to describe the orientation of the coin. A realistic mechanical model of the coin tossing is constructed in Section 4. It examines whether the initial states leading to heads or tails are distributed uniformly in phase space. The outcome of one trial from the given initial condition is determined via a following series of processes and conditions; (i) free fall process, i.e., the coin falls and rotates during the motion over the floor, (ii) contact condition which determines the moment at which the coin touches the floor, (iii) collision process (we assume that the force the coin receives from the floor is impulsive), (iv) stop condition which determines the moment after which the outcome of tossing is determined. We derive the equations of motion for the cases; (i) the imperfect coin, (ii) the ideal coin, (iii) the thin coin, (iv) 1D model of the coin. Section 5 shows numerical results of the simulation of the dynamics in several cases; (i) after the free fall the coin collides with a soft surface, (ii) the coin collides with a flat smooth surface (no friction between the coin and the floor surface), (iii) the coin collides with a rough surface (friction between the coin and the surface), (iv) with air resistance during free fall. Our results are compared with the results of Kechen [37], Mizuguchi and Suwashita [49] and Vulović and Prange [67] (Section 5.1). Section 5.2 presents basins of attraction of heads and tails (sets of initial conditions leading to both outcomes) which are calculated. It is shown that the boundaries between heads and tails domains are smooth. This allows us to state our main result that *there exists an open set of initial conditions for which the outcome of the coin tossing is predictable*. In Section 5.3 we point out that although heads and tails boundaries are smooth, the distance of a typical initial condition from a basin boundary is so small that practically any uncertainty (not infinitely small) in initial conditions can lead to the uncertainty of the result of tossing. Finally in Section 6 we summarize our results pointing out that the outcome of the coin tossing process is determined by the initial state.

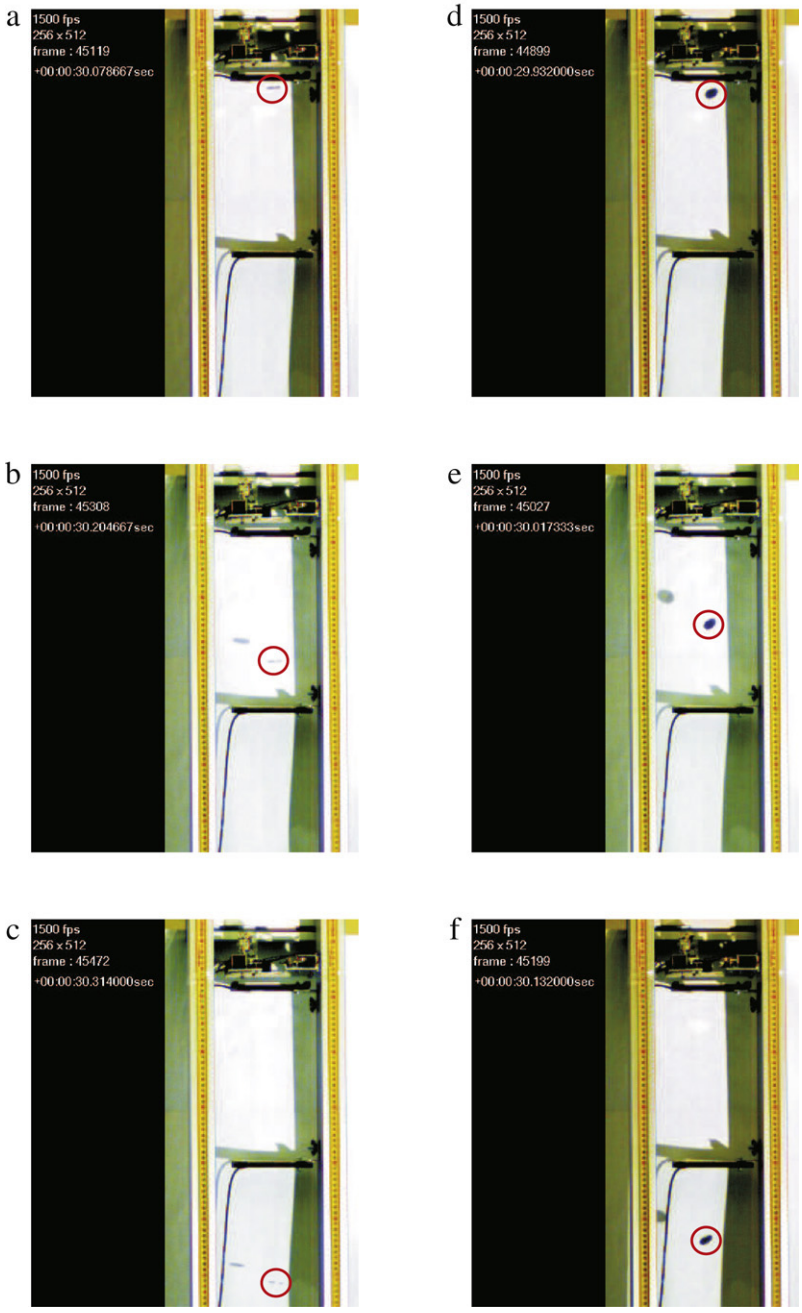

Fig. 3. Behavior of the coin during the free fall.

2. Experimental observations

We perform some simple laboratory experiments that allow for monitoring of the coin motion. The speed camera (Photron APX RS with the film speed at 1500 frames per second) has been used to observe the motion of a coin. We observed the tossing of two coins; a former Polish 1 zloty and a current British 2 pounds.

In the first experiment the coins have been released at the height of 186 cm by the special device which allows fixing the coin orientation at the beginning of motion. Examples of the coin motion during the free fall without rotation are shown in Fig. 3. In Fig. 3(a–c) at the initial moment the plane of the coin has been parallel to the floor and in Fig. 3(d–f) the angle between this plane and a floor has been fixed to $\pi/4$. One can notice the coin orientation is maintained during the motion and the side of the coin which has been up at the moment of release has not changed.

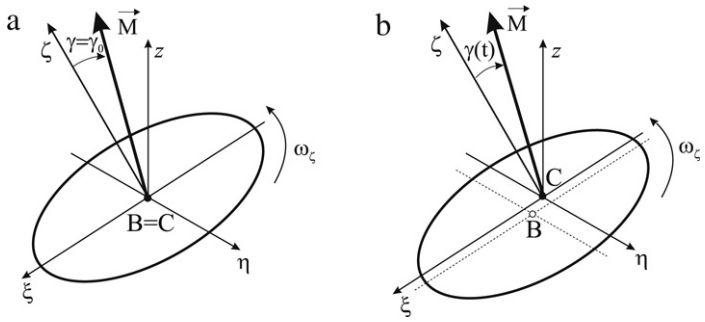

Fig. 4. The precessing coin: vector of angular momentum ($\vec{\mathbf{M}}$), upward direction (z) and normal (ζ) to the coin for: (a) ideal coin ($\gamma = \gamma_0 = \text{const}$), (b) imperfect coin ($\gamma = \gamma(t)$).

These experiments allow us to estimate the air resistance coefficients in normal and tangent directions (λ_n, λ_τ). For the former Polish 1 PLN coin these coefficients are equal respectively to $\lambda_n = 0.8$ and $\lambda_\tau = 0.2$. For details on air resistance see Section 4.2.

In other experiments (Figs. 5–7) we observe the coin motion with precession. The term precession is used to indicate that the direction of the axis of rotation changes as the coin goes through its trajectory [13]. The idea of precession is described in Fig. 4 where z indicates the upward direction, ζ is normal to the coin, $\vec{\mathbf{M}}$ is the angular momentum vector, and ω_ζ is the angular velocity around axis ζ. (In the motions presented in Fig. 3(a–f) there is no precession.)

In the study [13] it has been shown that for the ideal coin the angle γ between M and the normal to the coin is constant. One can see that if this angle is less than $\pi/4$ the coin never changes its face during the motion. The last observation allows magician and gamblers to perform such controlled tosses so that despite the fact that the toss looks fair the outcome is always determined.

In Figs. 5–7 we present a gallery of pictures describing the behavior of the coin after impacts against the floor. In this case the coin rotates around all possible axes, slides on the floor and can change its side during the motion between successive collisions. Our observations suggest that the bouncing of the coin on the floor introduces sensitive dependence of the final state (heads or tails) on the coin orientation at the moment of impact. The phenomena, which take place during the impacts can play a major role in the determination of the outcome of the toss. Generally the coin bouncing on the floor is less fair than the coin landing on the soft floor or caught in the hand.

3. Coin as a rigid body

A coin can be modeled as a rigid body, namely a cylinder with a radius r and height h as shown in Fig. 8. In the case of an ideal coin the geometrical center of the cylinder B and the center of the mass C coincide (i.e., $\xi_C = 0$, $\eta_C = 0$, $\zeta_C = 0$). For the imperfect coin the center of the mass is located at a certain distance from the geometrical center B ($\xi_C \neq 0$ or/and $\eta_C \neq 0$ or/and $\zeta_C \neq 0$).

Any arbitrary position of a rigid body with respect to the fixed reference frame $Oxyz$ (Fig. 10) can be described by a combination of the position of the origin of the local reference frame $x'y'z'$ and the orientation (angular position) of the frame $\xi\eta\zeta$. The local reference frame $x'y'z'$ is rigidly attached to the body and its axes are parallel to the xyz frame and $\xi\eta\zeta$ is the frame embedded and fixed in the body. It is convenient to choose the center of the mass (C) of the body or the geometric center (B) of the body model as the origin of the local frames. An imperfect coin is in fact a nonsymmetric body. Therefore to describe its motion we will use the geometric center (B) of the cylinder modeling the coin and the center of the mass (C) of the coin.

We present two alternative descriptions of the rigid body orientations, i.e., Euler angles [46,20,18,14,70,62,4] and Euler parameters [14,3]. If one uses Euler angles or similar conventions (known as Cardan angles and Tait–Bryan angles) in the dynamic analysis of a rigid body then some difficulties (singularities) can appear in the numerical solutions of equations of motion. The main advantage of Euler parameters (unit quaternions) is the lack of singularities in the numerical solutions of equations of 3D motion of a body. The problem of the tossed coin that starts with initial rotations around its axes (ξ, η, ζ) is one of the examples of such problems. In our studies a special emphasis is put on the formulation of equations of motion in quaternions.

3.1. Orientation of a rigid body

The orientation of a rigid body (orientation of a body embedded frame $\xi\eta\zeta$) with respect to the local reference frame $x'y'z'$ is described by [50,41,14,61]

$$\mathbf{r} = \mathbf{R}\,\mathbf{r}', \tag{1}$$

where:

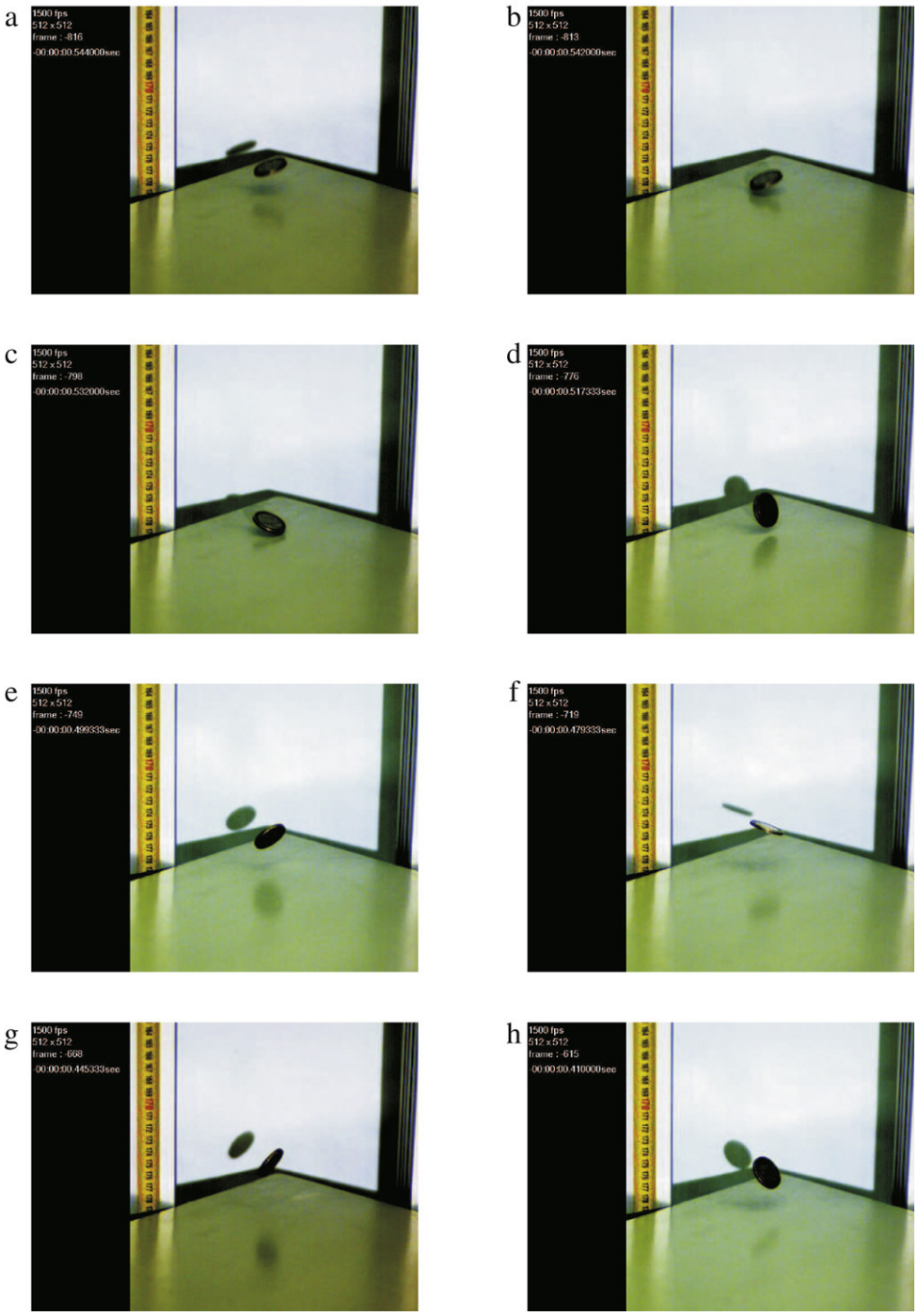

Fig. 5. Gallery of pictures presenting the behavior of the coin (British 2 pounds) during the impacts with the floor.

$\mathbf{r}$ — is the vector of coordinates representing the position of an arbitrary point A (Fig. 9) of the body before its rotation (in the initial position),
$\mathbf{r}'$ — is the vector of coordinates of the same point of the body after its rotation (in the final position),
$\mathbf{R}$ — is the rotation matrix (representing the orientation of the local frame $\xi\eta\zeta$, with respect to the frame $x'y'z'$).

The inverse transformation is defined by

$$\mathbf{r}' = \mathbf{R}^{-1}\,\mathbf{r} = \mathbf{R}^{\mathrm{T}}\,\mathbf{r}. \tag{2}$$

($\mathbf{R}^{-1}$ is the inverse matrix of $\mathbf{R}$, and $\mathbf{R}^{-1} = \mathbf{R}^{\mathrm{T}}$, whereas $\mathbf{R}^{\mathrm{T}}$ is the transpose matrix of $\mathbf{R}$).

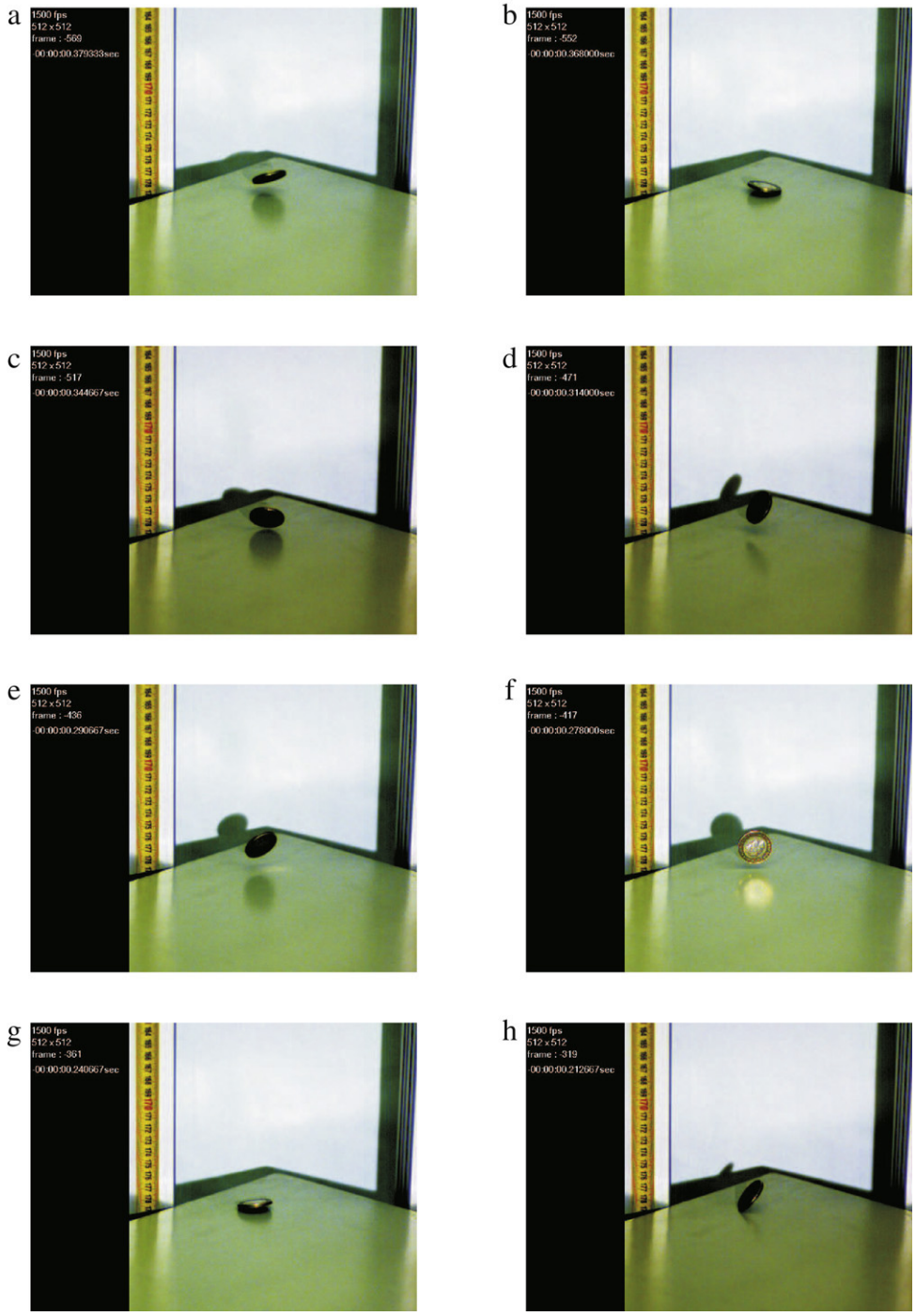

Fig. 6. Gallery of pictures presenting the behavior of the coin (British 2 pounds) during the impacts with the floor — continuation.

The matrix **R** can be expressed in different ways. Its form depends on coordinates that are chosen for the body orientation description. The elements of the rotation matrix (**R**) are cosines of the angles between the axes of body reference frames $x'y'z'$ and $\xi\eta\zeta$

$$\mathbf{R} = \begin{bmatrix} \cos\sphericalangle(x', \xi) & \cos\sphericalangle(x', \eta) & \cos\sphericalangle(x', \zeta) \\ \cos\sphericalangle(y', \xi) & \cos\sphericalangle(y', \eta) & \cos\sphericalangle(y', \zeta) \\ \cos\sphericalangle(z', \xi) & \cos\sphericalangle(z', \eta) & \cos\sphericalangle(z', \zeta) \end{bmatrix}. \tag{3}$$

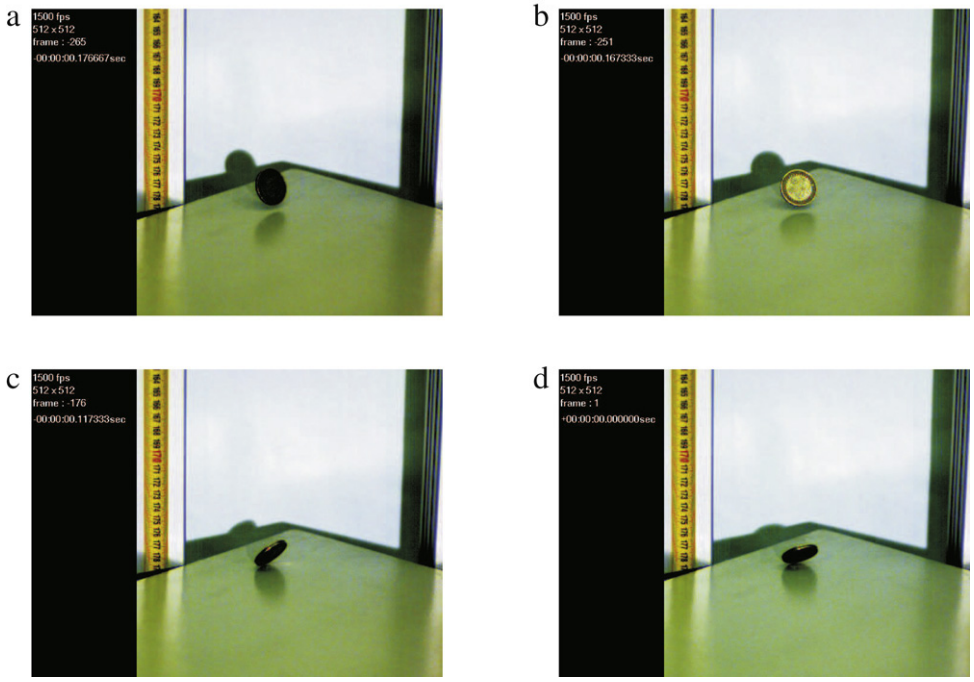

Fig. 7. Gallery of pictures presenting the behavior of the coin (British 2 pounds) during the impacts with the floor — continuation.

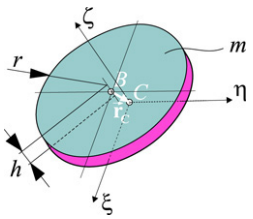

Fig. 8. 3D model of the imperfect coin.

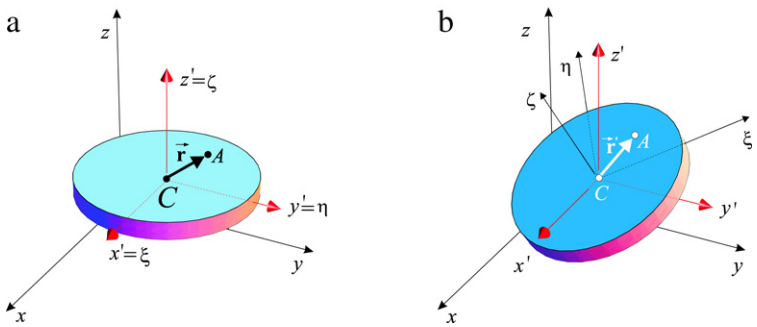

Fig. 9. Point A position vectors: (a) in the initial position — $\vec{\mathbf{r}}$, (b) in the final position — $\vec{\mathbf{r}}'$.

On the basis of the rotation matrix ($\mathbf{R}$) it is possible to define the matrix that contains the components of the body angular velocity vector (or angular velocity tensor) ($\boldsymbol{\Omega} = \dot{\mathbf{R}}\mathbf{R}^{\mathrm{T}}$), which is necessary in the dynamic analysis of the body. Matrix $\boldsymbol{\Omega}$ is obtained in the *xyz* reference frame. We use the symbol $\boldsymbol{\Omega}_{\xi}$ for the body angular velocity matrix defined by the components in the body embedded frame $\xi\eta\zeta$. This matrix is expressed as $\boldsymbol{\Omega}_{\xi} = \mathbf{R}^{\mathrm{T}}\boldsymbol{\Omega}\mathbf{R}$.

To determine whether the face of the coin which was directed upwards in the initial position, is directed upwards at the moment of the collision with the ground, it is necessary to determine the angle between z' and ζ axes. For the angles from the range $\langle -\pi/2, \pi/2\rangle$ the chosen side (i.e. the face expressed by equation $\zeta = h/2$ — say heads, or the face $\zeta = -h/2$ — tails)

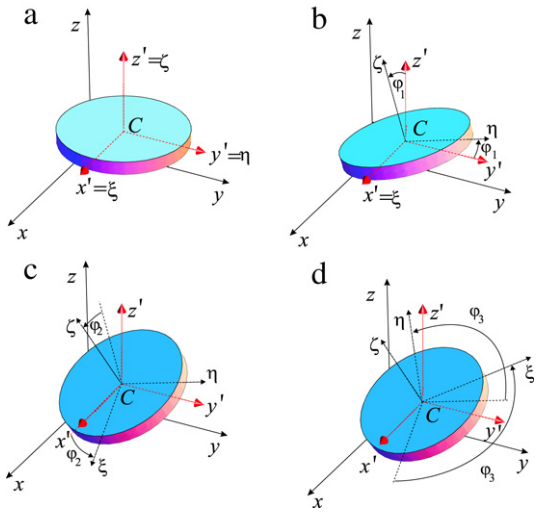

Fig. 10. Initial position of a coin (a) and the rotation sequence: φ_1 — around the ξ (b), φ_2 — around the η (c), φ_3 — around the ζ (d).

will be directed upwards. This corresponds to the following condition

$$\cos \sphericalangle(z', \zeta) > 0. \tag{4}$$

3.2. Euler angles and other conventions

In what follows, we adapt the conventions of [46,20,14,4] which are different from the ones used by [70]. Using Euler angles (or any other from 12 possible conventions of specifying the relative orientation of a body) the rotation matrix $\mathbf{R}$ is the composition of three consecutive rotations: φ_1, φ_2, φ_3, around axes $\xi\eta\zeta$ of the frame embedded and fixed in the body

$$\mathbf{R} = \mathbf{R}_1(\varphi_1)\mathbf{R}_2(\varphi_2)\mathbf{R}_3(\varphi_3), \tag{5}$$

whereas $\mathbf{R}_1(\varphi_1)$, $\mathbf{R}_2(\varphi_2)$, $\mathbf{R}_3(\varphi_3)$ are the matrices of successive rotations around ξ, η and ζ axes.

The definition of Euler angles is not unique. In works of various authors different sets of angles describe the body orientations and other naming conventions for the same angles are used. These conventions depend on the axes about which the rotations are carried out and on the rotation sequences. Basic definitions, names and expressions used in this work are briefly presented below. For the rotation of the body of value φ_i around the ξ axis (Fig. 10) the rotation matrix has the following form

$$\mathbf{R}_\xi(\varphi_i) = \begin{bmatrix} 1 & 0 & 0 \\ 0 & \cos\varphi_i & -\sin\varphi_i \\ 0 & \sin\varphi_i & \cos\varphi_i \end{bmatrix}. \tag{6}$$

For the rotation of value φ_i around the η axis

$$\mathbf{R}_\eta(\varphi_i) = \begin{bmatrix} \cos\varphi_i & 0 & \sin\varphi_i \\ 0 & 1 & 0 \\ -\sin\varphi_i & 0 & \cos\varphi_i \end{bmatrix}. \tag{7}$$

The rotation of value φ_i around the ζ axis leads to

$$\mathbf{R}_\zeta(\varphi_i) = \begin{bmatrix} \cos\varphi_i & -\sin\varphi_i & 0 \\ \sin\varphi_i & \cos\varphi_i & 0 \\ 0 & 0 & 1 \end{bmatrix}. \tag{8}$$

Depending on the order of rotations around the sequence of chosen axes there are 12 possible variants of this method of determining the position of a body in space. Denoting the axes $\xi\eta\zeta$ of the body embedded frame by symbols 1, 2, 3 ($\xi \to 1$, $\eta \to 2$, $\zeta \to 3$), possible rotation sequences can be represented as: 121 (ξ-η-ξ), 123 (ξ-η-ζ), 131 (ξ-ζ-ξ), 132 (ξ-ζ-η), 212 (η-ξ-η), 213 (η-ξ-ζ), 231 (η-ζ-ξ), 232 (η-ζ-η), 312 (ζ-ξ-η), 313 (ζ-ξ-ζ), 321 (ζ-η-ξ), 323 (ζ-η-ζ).

Classical Euler angles are: $\varphi_1 = \psi$, $\varphi_2 = \vartheta$, $\varphi_3 = \varphi$, that indicate consecutively the rotations: by angle $\varphi_1 = \psi$ around the ζ axis, by $\varphi_2 = \vartheta$ around the new position of the ξ axis, and by $\varphi_3 = \varphi$ around the ζ (rotation sequence is abbreviated as ζ-ξ-ζ or 313). The rotation matrix $\mathbf{R}$ for such angles is obtained by substituting the following rotational matrices to formula (5):

$$\mathbf{R}_1(\varphi_1) = \mathbf{R}_\zeta(\psi), \qquad \mathbf{R}_2(\varphi_2) = \mathbf{R}_\xi(\vartheta), \qquad \mathbf{R}_3(\varphi_3) = \mathbf{R}_\zeta(\varphi), \tag{9}$$

Table 1
Singularity condition in the numerical analysis of the rigid body dynamics ($k = 0, 1, \ldots$)

Rotation sequence	Singularity condition	Angle indicating singularity
121	$-\sin\varphi_2 = 0$	$\varphi_2 = \pm k\pi$
123	$\cos\varphi_2 = 0$	$\varphi_2 = \frac{\pi}{2} \pm k\pi$
131	$-\sin\varphi_2 = 0$	$\varphi_2 = \pm k\pi$
132	$-\cos\varphi_2 = 0$	$\varphi_2 = \frac{\pi}{2} \pm k\pi$
212	$-\sin\varphi_2 = 0$	$\varphi_2 = \pm k\pi$
213	$-\cos\varphi_2 = 0$	$\varphi_2 = \frac{\pi}{2} \pm k\pi$
231	$\cos\varphi_2 = 0$	$\varphi_2 = \frac{\pi}{2} \pm k\pi$
232	$-\sin\varphi_2 = 0$	$\varphi_2 = \pm k\pi$
312	$\cos\varphi_2 = 0$	$\varphi_2 = \frac{\pi}{2} \pm k\pi$
313	$-\sin\varphi_2 = 0$	$\varphi_2 = \pm k\pi$
321	$-\cos\varphi_2 = 0$	$\varphi_2 = \frac{\pi}{2} \pm k\pi$
323	$-\sin\varphi_2 = 0$	$\varphi_2 = \pm k\pi$

that means

$$\mathbf{R} = \mathbf{R}_\zeta(\psi)\mathbf{R}_\xi(\vartheta)\mathbf{R}_\zeta(\varphi). \tag{10}$$

In Table 1 the set of 12 possible rotation sequences as well as the singularity condition for each case and values of angles causing singularities in numerical solutions is presented. These singularities arise in the inversion process of the matrix $\mathbf{B}$, which is used to calculate the generalized velocities $\dot{\mathbf{q}}$ on the basis of body angular velocity $\boldsymbol{\omega}$ ($\dot{\mathbf{q}} = \mathbf{B}^{-1}\boldsymbol{\omega}$).

3.3. Euler parameters

An alternative to Euler angles and similar conventions of body orientation description are Euler parameters (also called Euler symmetric parameters and known in mathematics as normalized quaternions) [14,54,3]. They are very useful in representing the rotations due to some advantages in comparison to other representations. The main advantage of Euler parameters is that they do not produce any singularities in numerical solutions of body motion equations.

In the matrix notation Euler parameters are represented by the column matrix

$$\mathbf{p} = \begin{bmatrix} e_0 \\ e_1 \\ e_2 \\ e_3 \end{bmatrix} = \begin{bmatrix} \cos\dfrac{\phi}{2} \\ v_1 \sin\dfrac{\phi}{2} \\ v_2 \sin\dfrac{\phi}{2} \\ v_3 \sin\dfrac{\phi}{2} \end{bmatrix}, \tag{11}$$

or, shortly

$$\mathbf{p} = \begin{bmatrix} e_0 \\ \mathbf{e} \end{bmatrix} = \begin{bmatrix} \cos\dfrac{\phi}{2} \\ \mathbf{v} \sin\dfrac{\phi}{2} \end{bmatrix}. \tag{12}$$

The basis of this method of body orientation description is well known as the Euler theorem stating that any rotation of the rigid body can be expressed as a single rotation about some axis. The axis can be represented by a 3D vector $\vec{\mathbf{v}}$ (Fig. 11). The vector $\vec{\mathbf{v}}$ is a unit vector and it remains unchanged during the body rotation. The rotation angle ϕ is a scalar value.

The rotation matrix (3) can be expressed by Euler parameters as [54]

$$\mathbf{R} = (2e_0^2 - 1)\mathbf{I} + 2\mathbf{e}\mathbf{e}^{\mathrm{T}} + 2e_0\mathbf{E}, \tag{13}$$

in which $\mathbf{I}$ is the identity matrix of dimensions (3×3), and the matrix $\mathbf{E}$ has the form

$$\mathbf{E} = \begin{bmatrix} 0 & -e_3 & e_2 \\ e_3 & 0 & -e_1 \\ -e_2 & e_1 & 0 \end{bmatrix}. \tag{14}$$

The expanded form of the matrix $\mathbf{R}$ – expressed by unit quaternions $(e_0, \ldots, e_3)$ – has the following form (13)

$$\mathbf{R} = \begin{bmatrix} -1 + 2e_0^2 + 2e_1^2 & 2e_1e_2 - 2e_0e_3 & 2e_0e_2 + 2e_1e_3 \\ 2e_1e_2 + 2e_0e_3 & -1 + 2e_0^2 + 2e_2^2 & -2e_0e_1 + 2e_2e_3 \\ -2e_0e_2 + 2e_1e_3 & 2e_0e_1 + 2e_2e_3 & -1 + 2e_0^2 + 2e_3^2 \end{bmatrix}. \tag{15}$$

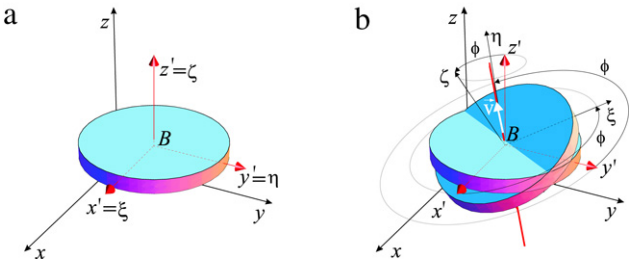

Fig. 11. The coin rotation by ϕ — around the vector $\vec{\mathbf{v}}$.

The antisymmetric matrix $\mathbf{\Omega}_\xi$ ($\mathbf{\Omega}_\xi = \mathbf{R}^{\mathrm{T}}\dot{\mathbf{R}}$) containing scalar components of the coin angular velocity vector – in the body embedded frame $\xi\eta\zeta$ – has the form

$$\mathbf{\Omega}_\xi = 2\begin{bmatrix} 0 & -\dot{e}_3e_0 + \dot{e}_2e_1 - \dot{e}_1e_2 + \dot{e}_0e_3 & \dot{e}_2e_0 + \dot{e}_3e_1 - \dot{e}_0e_2 - \dot{e}_1e_3 \\ & 0 & -\dot{e}_1e_0 + \dot{e}_0e_1 + \dot{e}_3e_2 - \dot{e}_2e_3 \\ & \textbf{\textit{asym}}. & 0 \end{bmatrix}. \tag{16}$$

The angular velocity vector of the coin $\boldsymbol{\omega}_\xi$ in the body embedded frame $\xi\eta\zeta$ is expressed by the column matrix

$$\boldsymbol{\omega}_\xi = \begin{bmatrix} \omega_\xi \\ \omega_\eta \\ \omega_\zeta \end{bmatrix} = 2\begin{bmatrix} \dot{e}_1e_0 - \dot{e}_0e_1 - \dot{e}_3e_2 + \dot{e}_2e_3 \\ \dot{e}_2e_0 + \dot{e}_3e_1 - \dot{e}_0e_2 - \dot{e}_1e_3 \\ \dot{e}_3e_0 - \dot{e}_2e_1 + \dot{e}_1e_2 - \dot{e}_0e_3 \end{bmatrix}, \tag{17}$$

whereas

$$\dot{\boldsymbol{\omega}}_\xi = \begin{bmatrix} \dot{\omega}_\xi \\ \dot{\omega}_\eta \\ \dot{\omega}_\zeta \end{bmatrix} = 2\begin{bmatrix} -e_1\ddot{e}_0 + e_0\ddot{e}_1 + e_3\ddot{e}_2 - e_2\ddot{e}_3 \\ -e_2\ddot{e}_0 - e_3\ddot{e}_1 + e_0\ddot{e}_2 + e_1\ddot{e}_3 \\ -e_3\ddot{e}_0 + e_2\ddot{e}_1 - e_1\ddot{e}_2 + e_0\ddot{e}_3 \end{bmatrix}. \tag{18}$$

The column matrix containing xyz scalar components of the coin angular velocity vector (i.e. the components in fixed spatial frame) has the form

$$\boldsymbol{\omega} = \begin{bmatrix} \omega_x \\ \omega_y \\ \omega_z \end{bmatrix} = 2\begin{bmatrix} \dot{e}_1e_0 - \dot{e}_0e_1 + \dot{e}_3e_2 - \dot{e}_2e_3 \\ \dot{e}_2e_0 - \dot{e}_3e_1 - \dot{e}_0e_2 + \dot{e}_1e_3 \\ \dot{e}_3e_0 + \dot{e}_2e_1 - \dot{e}_1e_2 - \dot{e}_0e_3 \end{bmatrix}. \tag{19}$$

Using Euler parameters allows avoiding singularities in numerical solutions of body rotation problems. The coin dynamics is one of such problems. The equations of coin dynamics are presented in the following sections. Special attention is paid to the body dynamics description in quaternions.

4. The dynamics of a tossed coin

In our studies we consider the following motion of the coin. We assume that the coin is thrown at the height z_0 (the mass center initial position vector $\mathbf{r}_{(t=0)} = [\ x_0\ \ y_0\ \ z_0\ ]^{\mathrm{T}}$, coin initial orientation $\boldsymbol{\psi}_{(t=0)} = [\ \psi_0\ \ \theta_0\ \ \varphi_0\ ]^{\mathrm{T}}$ with the initial angular velocity $\boldsymbol{\omega}_{\xi\,(t=0)} = [\ \omega_{\xi 0}\ \ \omega_{\eta 0}\ \ \omega_{\zeta 0}\ ]^{\mathrm{T}}$ and the mass center initial velocity $\mathbf{v}_{C\,(t=0)} = [\ \dot{x}_0\ \ \dot{y}_0\ \ \dot{z}_0\ ]^{\mathrm{T}}$. After a free fall when the z coordinate of one of coin points is equal to zero, say $z_D = 0$ the coin collides with the horizontal base (floor). It is assumed that at the collision a portion of the coin energy is dissipated, i.e., the collision is described by the restitution coefficient $\chi < 1$. After the collision, the coin mass center moves to the height z_1 in which the total mechanical energy of the coin $E = T + V$ is equal its total energy in the moment after the collision $E' = T' + V'$. (In the case when air resistance is taken into account total mechanical energy of the coin at height z_1 is less then its value after the collision $E < E'$.) Next, the coin moves on until it collides with the floor again. The calculations are terminated when after the nth collision the total mechanical energy of the coin $E = T + V$ is smaller than the potential energy at the coin center level equal to its radius r, i.e $E < mgr$, as this condition disables the change of the coin face during the further motion. The no-turning-over condition $E < mgr$ can be modified in particular cases of the coin–base collision model. For example, for symmetric, perfectly smooth – frictionless – coin and base the condition is $E(z, \dot{z},\ \omega_\xi,\ \omega_\eta) < mgr$, which means that only the part of kinetic energy is taken into account i.e. the term $\frac{1}{2}J_\zeta{\omega_\zeta}^2$ is neglected. This improved criterion has the form

$$T + V - \frac{1}{2}(m\dot{x}^2 + m\dot{y}^2 + J_\zeta{\omega_\zeta}^2) < mgr. \tag{20}$$

We derive the equations of motion for the cases of imperfect and ideal coins, i.e. the equations describing the motion of 3D rigid body in the 3D space for nonsymmetric and symmetric bodies. Additionally the simplified models of 2D coin (thin disk, $h = 0$) in the space motion, and 1D coin model — disk performing planar motion in the vertical plane are considered. (It should be mentioned here that our 1D model in [67,49] was called the 2D one.)

4.1. Free fall

The rigid body dynamics equations can be expressed as two equations in the matrix form that describe:

- the acceleration of the body mass center (and its position)

$$\mathbf{M}\mathbf{a}_C = \mathbf{f}, \tag{21}$$

- the changes of the body angular velocity (and in the body orientation)

$$\mathbf{J}_C\dot{\boldsymbol{\omega}}_\xi + \boldsymbol{\Omega}_\xi\mathbf{J}_C\boldsymbol{\omega}_\xi = \mathbf{m}_C. \tag{22}$$

In the mentioned equations $\mathbf{M}$ is the mass matrix of coin ($\mathbf{M} = \text{diag}\,[m\ \ m\ \ m]$), $\mathbf{a}_C$ is the vector (column matrix) of the body mass center (the point C) absolute acceleration, $\mathbf{f}$ contains the components of the body force vector, $\mathbf{J}_C$ is the body moment of inertia matrix (determined with respect to the body embedded frame $\xi_C\eta_C\zeta_C$), $\boldsymbol{\omega}_\xi$ and $\boldsymbol{\Omega}_\xi$ are the body angular velocity vector in the form of the column matrix and antisymmetric matrix, and $\mathbf{m}_C$ is the column matrix of external force moments with respect to the mass center C.

The column matrices $\mathbf{a}_C$ and $\mathbf{f}$ are expressed by vector components with respect to the fixed frame (xyz): $\mathbf{a}_C = [\ddot{x}\ \ddot{y}\ \ddot{z}]^{\mathrm{T}}$, $\mathbf{f} = [f_x\ f_y\ f_z]^{\mathrm{T}}$. On the other hand, it is more convenient to describe the rotations of the body (Eq. (22)) by their components with respect to the body embedded frame ($\xi\eta\zeta$).

Eqs. (21) and (22) are general equations of motion and are suitable for the dynamics analysis of any body i.e. a nonsymmetric and nonhomogeneous body. In the case in which the forces $\mathbf{f}$ are independent of the angular velocity of the body and moments $\mathbf{m}_C$ are not the functions of the center of mass accelerations Eqs. (21) and (22) are uncoupled. This happens when air resistance is neglected.

In the case of a cylinder shaped coin (or modeled by the cylindrical body) of homogeneous material its center of mass (point C) is situated in the geometrical center of the cylinder (in point B). The body embedded frame axes (ξ, η, ζ) are the axes passing through the center of the mass. As the products of inertia are zeros these axes are the central axes, and the inertia matrix of the coin ($\mathbf{J}_C$) is a diagonal matrix.

For an imperfect (nonsymmetric or nonhomogeneous) coin the points B and C are not overlapping. For such a case, it can be more convenient to use the following form of body dynamics equations:

$$\mathbf{M}(\mathbf{a}_B + \dot{\boldsymbol{\Omega}}\mathbf{r}_C + \boldsymbol{\Omega}\boldsymbol{\Omega}\mathbf{r}_C) = \mathbf{f}, \tag{23}$$

$$\mathbf{J}_B\dot{\boldsymbol{\omega}}_\xi + \boldsymbol{\Omega}_\xi\mathbf{J}_B\boldsymbol{\omega}_\xi + \mathbf{M}\mathbf{R}_C\mathbf{a}_B = \mathbf{m}_B, \tag{24}$$

where: $\mathbf{a}_B$ denotes the point B absolute acceleration, $\mathbf{r}_C$ and $\mathbf{R}_C$ include coordinates of the vector $\vec{\mathbf{r}}_C$, describing the position of mass center (C) with respect to the origin B, $\mathbf{J}_B$ is the body moment of inertia matrix (determined with respect to the body embedded frame $\xi_B\eta_B\zeta_B$ − parallel to the $\xi\eta\zeta$ and with origin in B), and $\mathbf{m}_B$ is the body force moment with respect to the point B. In the general case, for a nonsymmetric or nonhomogeneous coin, the matrix $\mathbf{J}_B$ will not be diagonal, because the axes $B\xi$, $B\eta$, $B\zeta$ will not be principal axes (some nonzero inertia products in $\mathbf{J}_B$ will appear).

Unlike (21) and (22) Eqs. (23) and (24) are coupled equations.

The scalar form of body dynamics equations obtained from the general equations (21) and (22) can be written in the well-known form of the Newton–Euler equations:

$$m\ddot{x} = f_x, \qquad m\ddot{y} = f_y, \qquad m\ddot{z} = f_z, \tag{25}$$

and

$$J_\xi\dot{\omega}_\xi + \left(J_\zeta - J_\eta\right)\omega_\eta\omega_\zeta - J_{\xi\zeta}\dot{\omega}_\zeta - J_{\xi\eta}\dot{\omega}_\eta + J_{\eta\zeta}\left(\omega_\zeta{}^2 - \omega_\eta{}^2\right) + \left(J_{\xi\eta}\omega_\zeta - J_{\xi\zeta}\omega_\eta\right)\omega_\xi = M_\xi, \tag{26}$$

$$J_\eta\dot{\omega}_\eta + \left(J_\xi - J_\zeta\right)\omega_\xi\omega_\zeta - J_{\xi\eta}\dot{\omega}_\xi - J_{\eta\zeta}\dot{\omega}_\zeta + J_{\xi\zeta}\left(\omega_\xi{}^2 - \omega_\zeta{}^2\right) + \left(J_{\eta\zeta}\omega_\xi - J_{\xi\eta}\omega_\zeta\right)\omega_\eta = M_\eta, \tag{27}$$

$$J_\zeta\dot{\omega}_\zeta + \left(J_\eta - J_\xi\right)\omega_\xi\omega_\eta - J_{\eta\zeta}\dot{\omega}_\eta - J_{\xi\zeta}\dot{\omega}_\xi + J_{\xi\eta}\left(\omega_\eta{}^2 - \omega_\xi{}^2\right) + \left(J_{\xi\zeta}\omega_\eta - J_{\eta\zeta}\omega_\xi\right)\omega_\zeta = M_\zeta. \tag{28}$$

(The moments of inertia in this case are determined with respect to the body embedded frame $\xi\eta\zeta$ with the origin in the mass center.)

Expressing ω_ξ, ω_η, ω_ζ in terms of Euler angles (φ, ϑ, ψ) or in normalized quaternions (e_0, e_1, e_2, e_3) one can obtain the motion equations in the chosen coordinates.

The full equations of motion for the cases of (i) imperfect, (ii) ideal 3D coin as well as for (iii) two- and (iv) 1D coin models are shown below. In all equations Euler parameters (normalized quaternions) have been applied.

(i) Equations of motion of imperfect coin.

The first three scalar equations obtained from the general equation (21) are common for all coin models:

$$m\ddot{x} = f_x, \qquad m\ddot{y} = f_y, \qquad m\ddot{z} = f_z. \tag{29}$$

If the air resistance of a coin is taken into account then all force components (f_x, f_y, f_z) have nonzero values. (Air resistance forces and their moments are derived in the next section.) In the case of free fall of a body the component f_z is the only force acting on the coin ($f_{zg} = -mg$).

The equations describing the changes in the spatial orientation of the coin obtained from (22), expressed in Euler parameters, have the following form:

$$
\begin{aligned}
&2\left((-e_1\dot{e}_0+e_0\dot{e}_1+e_3\dot{e}_2-e_2\dot{e}_3)\left(2J_{\xi\eta}\left(-e_3\dot{e}_0+e_2\dot{e}_1-e_1\dot{e}_2+e_0\dot{e}_3\right)+2J_{\xi\zeta}\left(e_2\dot{e}_0+e_3\dot{e}_1-e_0\dot{e}_2-e_1\dot{e}_3\right)\right)\right.\\
&\quad+\left(-e_3\dot{e}_0+e_2\dot{e}_1-e_1\dot{e}_2+e_0\dot{e}_3\right)\left(2J_{\eta\zeta}\left(-e_3\dot{e}_0+e_2\dot{e}_1-e_1\dot{e}_2+e_0\dot{e}_3\right)+2J_{\zeta}\left(-e_2\dot{e}_0-e_3\dot{e}_1+e_0\dot{e}_2+e_1\dot{e}_3\right)\right)\\
&\quad-\left(-e_2\dot{e}_0-e_3\dot{e}_1+e_0\dot{e}_2+e_1\dot{e}_3\right)\left(2J_{\eta}\left(-e_3\dot{e}_0+e_2\dot{e}_1-e_1\dot{e}_2+e_0\dot{e}_3\right)+2J_{\eta\zeta}\left(-e_2\dot{e}_0-e_3\dot{e}_1+e_0\dot{e}_2+e_1\dot{e}_3\right)\right)\\
&\quad\left.+J_{\xi\zeta}\left(e_3\ddot{e}_0-e_2\ddot{e}_1+e_1\ddot{e}_2-e_0\ddot{e}_3\right)+J_{\xi\eta}\left(e_2\ddot{e}_0+e_3\ddot{e}_1-e_0\ddot{e}_2-e_1\ddot{e}_3\right)+J_{\xi}\left(-e_1\ddot{e}_0+e_0\ddot{e}_1+e_3\ddot{e}_2-e_2\ddot{e}_3\right)\right)=M_{\xi},
\end{aligned}
\tag{30}
$$

$$
\begin{aligned}
&4J_{\zeta}\left(e_3\dot{e}_0-e_2\dot{e}_1+e_1\dot{e}_2-e_0\dot{e}_3\right)\left(-e_1\dot{e}_0+e_0\dot{e}_1+e_3\dot{e}_2-e_2\dot{e}_3\right)\\
&\quad+4J_{\xi}\left(-e_3\dot{e}_0+e_2\dot{e}_1-e_1\dot{e}_2+e_0\dot{e}_3\right)\left(-e_1\dot{e}_0+e_0\dot{e}_1+e_3\dot{e}_2-e_2\dot{e}_3\right)\\
&\quad+4J_{\eta\zeta}\left(e_2\dot{e}_0+e_3\dot{e}_1-e_0\dot{e}_2-e_1\dot{e}_3\right)\left(e_1\dot{e}_0-e_0\dot{e}_1-e_3\dot{e}_2+e_2\dot{e}_3\right)\\
&\quad+J_{\xi\zeta}\left(-4\left(e_3\dot{e}_0-e_2\dot{e}_1+e_1\dot{e}_2-e_0\dot{e}_3\right)^2+4\left(e_1\dot{e}_0-e_0\dot{e}_1-e_3\dot{e}_2+e_2\dot{e}_3\right)^2\right)+2J_{\eta\zeta}\left(e_3\ddot{e}_0-e_2\ddot{e}_1+e_1\ddot{e}_2-e_0\ddot{e}_3\right)\\
&\quad+2J_{\eta}\left(-e_2\ddot{e}_0-e_3\ddot{e}_1+e_0\ddot{e}_2+e_1\ddot{e}_3\right)-2J_{\xi\eta}\left(2\left(e_3\dot{e}_0-e_2\dot{e}_1+e_1\dot{e}_2-e_0\dot{e}_3\right)\left(e_2\dot{e}_0+e_3\dot{e}_1-e_0\dot{e}_2-e_1\dot{e}_3\right)\right.\\
&\quad\left.-e_1\ddot{e}_0+e_0\ddot{e}_1+e_3\ddot{e}_2-e_2\ddot{e}_3\right)=M_{\eta},
\end{aligned}
\tag{31}
$$

$$
\begin{aligned}
&2\left((-e_2\dot{e}_0-e_3\dot{e}_1+e_0\dot{e}_2+e_1\dot{e}_3)\left(2J_{\xi\eta}\left(-e_2\dot{e}_0-e_3\dot{e}_1+e_0\dot{e}_2+e_1\dot{e}_3\right)+2J_{\eta}\left(-e_1\dot{e}_0+e_0\dot{e}_1+e_3\dot{e}_2-e_2\dot{e}_3\right)\right)\right.\\
&\quad-\left(-e_1\dot{e}_0+e_0\dot{e}_1+e_3\dot{e}_2-e_2\dot{e}_3\right)\left(2J_{\xi}\left(-e_2\dot{e}_0-e_3\dot{e}_1+e_0\dot{e}_2+e_1\dot{e}_3\right)+2J_{\xi\eta}\left(-e_1\dot{e}_0+e_0\dot{e}_1+e_3\dot{e}_2-e_2\dot{e}_3\right)\right)\\
&\quad+\left(-e_3\dot{e}_0+e_2\dot{e}_1-e_1\dot{e}_2+e_0\dot{e}_3\right)\left(2J_{\xi\zeta}\left(-e_2\dot{e}_0-e_3\dot{e}_1+e_0\dot{e}_2+e_1\dot{e}_3\right)+2J_{\eta\zeta}\left(e_1\dot{e}_0-e_0\dot{e}_1-e_3\dot{e}_2+e_2\dot{e}_3\right)\right)\\
&\quad\left.+J_{\zeta}\left(-e_3\ddot{e}_0+e_2\ddot{e}_1-e_1\ddot{e}_2+e_0\ddot{e}_3\right)+J_{\eta\zeta}\left(e_2\ddot{e}_0+e_3\ddot{e}_1-e_0\ddot{e}_2-e_1\ddot{e}_3\right)+J_{\xi\zeta}\left(e_1\ddot{e}_0-e_0\ddot{e}_1-e_3\ddot{e}_2+e_2\ddot{e}_3\right)\right)=M_{\zeta}.
\end{aligned}
\tag{32}
$$

The right-hand-side quantities (M_{ξ}, M_{η}, M_{ζ}) denote the moments of air resistance forces with respect to the body embedded axes (central axes $C\xi$, $C\eta$, $C\zeta$). The formulae defining these moments for 3D imperfect coin model in the general form ($\mathbf{m}_C=[M_{\xi}\ \ M_{\eta}\ \ M_{\zeta}]^{\mathrm{T}}$) as well as for particular coin models are presented in Section 4.2.

The additional equation that has to be satisfied in the case when Euler parameters are used as coordinates takes the following form:

$$
\dot{e}_0^2+\dot{e}_1^2+\dot{e}_2^2+\dot{e}_3^2+e_0\ddot{e}_0+e_1\ddot{e}_1+e_2\ddot{e}_2+e_3\ddot{e}_3=0. \tag{33}
$$

(ii) Equations of motion of an ideal coin.

The equations describing the changes in the spatial orientation of the symmetrical coin obtained from (30)–(32) for $J_{\xi}=J_{\eta}=\frac{mr^2}{4}+\frac{mh^2}{12}$, $J_{\zeta}=\frac{mr^2}{2}$ and $J_{\xi\eta}=J_{\eta\zeta}=J_{\zeta\xi}=0$, expressed with Euler parameters, are as follows:

$$
\begin{aligned}
&2\left(mr^2\left(e_3\dot{e}_0-e_2\dot{e}_1+e_1\dot{e}_2-e_0\dot{e}_3\right)\left(e_2\dot{e}_0+e_3\dot{e}_1-e_0\dot{e}_2-e_1\dot{e}_3\right)\right.\\
&\quad-\frac{1}{6}m\left(h^2+3r^2\right)\left(e_3\dot{e}_0-e_2\dot{e}_1+e_1\dot{e}_2-e_0\dot{e}_3\right)\left(e_2\dot{e}_0+e_3\dot{e}_1-e_0\dot{e}_2-e_1\dot{e}_3\right)\\
&\quad\left.-\frac{1}{12}m\left(h^2+3r^2\right)\left(e_1\ddot{e}_0-e_0\ddot{e}_1-e_3\ddot{e}_2+e_2\ddot{e}_3\right)\right)=M_{\xi},
\end{aligned}
\tag{34}
$$

$$
\begin{aligned}
&\frac{1}{6}m\left(12r^2\left(e_3\dot{e}_0-e_2\dot{e}_1+e_1\dot{e}_2-e_0\dot{e}_3\right)\left(-e_1\dot{e}_0+e_0\dot{e}_1+e_3\dot{e}_2-e_2\dot{e}_3\right)\right.\\
&\quad+2\left(h^2+3r^2\right)\left(e_3\dot{e}_0-e_2\dot{e}_1+e_1\dot{e}_2-e_0\dot{e}_3\right)\left(e_1\dot{e}_0-e_0\dot{e}_1-e_3\dot{e}_2+e_2\dot{e}_3\right)\\
&\quad\left.-\left(h^2+3r^2\right)\left(e_2\ddot{e}_0+e_3\ddot{e}_1-e_0\ddot{e}_2-e_1\ddot{e}_3\right)\right)=M_{\eta},
\end{aligned}
\tag{35}
$$

$$
\begin{aligned}
&\frac{1}{3}m\left(\left(h^2+3r^2\right)\left(e_3\dot{e}_0-e_2\dot{e}_1+e_1\dot{e}_2-e_0\dot{e}_3\right)\left(e_2\dot{e}_0+e_3\dot{e}_1-e_0\dot{e}_2-e_1\dot{e}_3\right)\right.\\
&\quad+\left(h^2+3r^2\right)\left(e_2\dot{e}_0+e_3\dot{e}_1-e_0\dot{e}_2-e_1\dot{e}_3\right)\left(-e_1\dot{e}_0+e_0\dot{e}_1+e_3\dot{e}_2-e_2\dot{e}_3\right)\\
&\quad\left.+3r^2\left(-e_3\ddot{e}_0+e_2\ddot{e}_1-e_1\ddot{e}_2+e_0\ddot{e}_3\right)\right)=M_{\zeta}.
\end{aligned}
\tag{36}
$$

(iii) Equations of a 2D coin model.

For the 2D ($h=0$) imperfect coin model the products of inertia $J_{\eta\zeta}=0$ and $J_{\zeta\xi}=0$ are used in (30)–(32). Only one off-diagonal element of a coin inertia matrix remains nonzero ($J_{\xi\eta}\neq 0$). After these substitutions:

$$
\begin{aligned}
&2\left(2J_{\zeta}\left(-e_3\dot{e}_0+e_2\dot{e}_1-e_1\dot{e}_2+e_0\dot{e}_3\right)\left(-e_2\dot{e}_0-e_3\dot{e}_1+e_0\dot{e}_2+e_1\dot{e}_3\right)\right.\\
&\quad\left.-2J_{\eta}\left(-e_3\dot{e}_0+e_2\dot{e}_1-e_1\dot{e}_2+e_0\dot{e}_3\right)\left(-e_2\dot{e}_0-e_3\dot{e}_1+e_0\dot{e}_2+e_1\dot{e}_3\right)\right.
\end{aligned}
$$

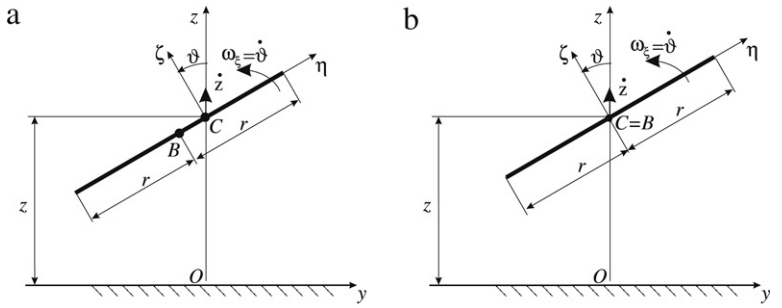

Fig. 12. 1D coin models (yz projection): (a) an imperfect coin, (b) an ideal coin.

$$+2J_{\xi\eta}\left(-e_3\dot{e}_0+e_2\dot{e}_1-e_1\dot{e}_2+e_0\dot{e}_3\right)\left(-e_1\dot{e}_0+e_0\dot{e}_1+e_3\dot{e}_2-e_2\dot{e}_3\right)$$
$$+J_{\xi\eta}\left(e_2\ddot{e}_0+e_3\ddot{e}_1-e_0\ddot{e}_2-e_1\ddot{e}_3\right)+J_{\xi}\left(-e_1\ddot{e}_0+e_0\ddot{e}_1+e_3\ddot{e}_2-e_2\ddot{e}_3\right)\Big)=M_{\xi}, \tag{37}$$
$$4J_{\zeta}\left(e_3\dot{e}_0-e_2\dot{e}_1+e_1\dot{e}_2-e_0\dot{e}_3\right)\left(-e_1\dot{e}_0+e_0\dot{e}_1+e_3\dot{e}_2-e_2\dot{e}_3\right)$$
$$+4J_{\xi}\left(-e_3\dot{e}_0+e_2\dot{e}_1-e_1\dot{e}_2+e_0\dot{e}_3\right)\left(-e_1\dot{e}_0+e_0\dot{e}_1+e_3\dot{e}_2-e_2\dot{e}_3\right)+2J_{\eta}\left(-e_2\ddot{e}_0-e_3\ddot{e}_1+e_0\ddot{e}_2+e_1\ddot{e}_3\right)$$
$$-2J_{\xi\eta}\left(2\left(e_3\dot{e}_0-e_2\dot{e}_1+e_1\dot{e}_2-e_0\dot{e}_3\right)\left(e_2\dot{e}_0+e_3\dot{e}_1-e_0\dot{e}_2-e_1\dot{e}_3\right)-e_1\ddot{e}_0+e_0\ddot{e}_1+e_3\ddot{e}_2-e_2\ddot{e}_3\right)=M_{\eta}, \tag{38}$$
$$4J_{\eta}\left(e_3\dot{e}_0-e_2\dot{e}_1+e_1\dot{e}_2-e_0\dot{e}_3\right)\left(e_2\dot{e}_0+e_3\dot{e}_1-e_0\dot{e}_2-e_1\dot{e}_3\right)+4J_{\xi\eta}\left(e_2\dot{e}_0+e_3\dot{e}_1-e_0\dot{e}_2-e_1\dot{e}_3\right)^2$$
$$+4J_{\xi\eta}\left(e_3\dot{e}_0-e_2\dot{e}_1+e_1\dot{e}_2-e_0\dot{e}_3\right)\left(-e_1\dot{e}_0+e_0\dot{e}_1+e_3\dot{e}_2-e_2\dot{e}_3\right)$$
$$+4J_{\xi}\left(e_2\dot{e}_0+e_3\dot{e}_1-e_0\dot{e}_2-e_1\dot{e}_3\right)\left(-e_1\dot{e}_0+e_0\dot{e}_1+e_3\dot{e}_2-e_2\dot{e}_3\right)+2J_{\zeta}\left(-e_3\ddot{e}_0+e_2\ddot{e}_1-e_1\ddot{e}_2+e_0\ddot{e}_3\right)=M_{\zeta}. \tag{39}$$

(iv) Equations of a 1D coin model.

Let us assume that the coin is thin ($h=0, J_{\xi\zeta}=J_{\eta\zeta}=0$), it rotates only around the ξ axis ($\omega_{\eta}=\omega_{\zeta}=0$ and $\dot{\omega}_{\eta}=\dot{\omega}_{\zeta}=0$), which means that ξ remains horizontal during motion. In this case one obtains a 1D model of the coin shown in Fig. 6 and general equations (29)–(32) can be simplified as follows:

$$m\ddot{x}=f_x,\qquad m\ddot{y}=f_y,\qquad m\ddot{z}=f_z, \tag{40}$$
$$2J_{\xi}\left(-e_1\ddot{e}_0+e_0\ddot{e}_1+e_3\ddot{e}_2-e_2\ddot{e}_3\right)=M_{\xi}, \tag{41}$$
$$-2J_{\xi\eta}\left(-e_1\ddot{e}_0+e_0\ddot{e}_1+e_3\ddot{e}_2-e_2\ddot{e}_3\right)=M_{\eta}, \tag{42}$$
$$-4J_{\xi\eta}\left(e_1\dot{e}_0-e_0\dot{e}_1-e_3\dot{e}_2+e_2\dot{e}_3\right)^2=M_{\zeta}. \tag{43}$$

It is possible to show that the last three equations are identical with: $J_{\xi}\ddot{\vartheta}=M_{\xi}$, $-J_{\xi\eta}\ddot{\vartheta}=M_{\eta}$, $0=M_{\zeta}$, i.e. with the dynamic equations describing rotations of a rigid body ($J_{\xi\zeta}=J_{\eta\zeta}=0$) in plane motion – expressed in rotation angle ϑ (one of the Euler angles). In this case the body rotates by ϑ about the ξ axis parallel to x which means that the rotation angle ϕ is equal to ϑ ($\phi=\vartheta$) and the unit vector $\vec{\mathbf{v}}$ has the x axis direction ($v_1=1, v_2=0, v_3=0$). Euler parameters (11) are as follows:

$$\mathbf{p}=\begin{bmatrix}e_0\\e_1\\e_2\\e_3\end{bmatrix}=\begin{bmatrix}\cos\dfrac{\vartheta}{2}\\v_1\sin\dfrac{\vartheta}{2}\\0\\0\end{bmatrix}. \tag{44}$$

Substituting $e_0=\cos\frac{\vartheta}{2}$, $e_1=\sin\frac{\vartheta}{2}$, $e_2=e_3=0$ in (41)–(43) leads to

$$-e_1\ddot{e}_0+e_0\ddot{e}_1+e_3\ddot{e}_2-e_2\ddot{e}_3=\frac{\ddot{\vartheta}}{2}\left(\sin^2\frac{\vartheta}{2}+\cos^2\frac{\vartheta}{2}\right)=\frac{\ddot{\vartheta}}{2}, \tag{45}$$
$$e_1\dot{e}_0-e_0\dot{e}_1-e_3\dot{e}_2+e_2\dot{e}_3=-\frac{\dot{\vartheta}}{2}\left(\sin^2\frac{\vartheta}{2}+\cos^2\frac{\vartheta}{2}\right)=-\frac{\dot{\vartheta}}{2}, \tag{46}$$

hence

$$J_{\xi}\ddot{\vartheta}=M_{\xi},\qquad -J_{\xi\eta}\ddot{\vartheta}=M_{\eta},\qquad -J_{\xi\eta}\dot{\vartheta}^2=M_{\zeta}. \tag{47}$$

In Fig. 12 1D models of an imperfect coin and an ideal coin are shown.

Assuming that the coin is symmetric with respect to the $\eta\zeta$ plane ($J_{\xi\eta} = 0$) we find the dynamic equations of the plane motion of the coin in the form:

$$\begin{aligned} &m\ddot{x} = f_x, \qquad m\ddot{y} = f_y, \qquad m\ddot{z} = f_z \\ &J_\xi\ddot{\vartheta} = M_\xi, \qquad 0 = M_\eta, \qquad 0 = M_\zeta. \end{aligned} \tag{48}$$

It should be mentioned here that although in a 1D model the coin reminds us of a bar (as in Fig. 12) in Eq. (48) one has to consider the moment of inertia for cylinder or disk, i.e., $J_\xi = \frac{mr^2}{4} + \frac{mh^2}{12}$ or $J_\eta = \frac{mr^2}{4}$. Considering bar moment of inertia $J_\xi = J_\eta = \frac{ml^2}{12}$ in Eq. (48) one solves the problem of the plane motion of the bar [67,49]. Such models can be used in the discussion of the mechanical randomizers but cannot be used as models of a tossed coin.

4.2. Forces and moments due to the air resistance

To define the right-hand sides of Eqs. (21)–(22), and (23)–(24) the components of the forces acting on the body and moments of these forces with respect to the $B\xi\eta\zeta$ frame axis should be determined.

The determination of the air resistance forces acting on the coin is cumbersome due to its variable velocity and a change in the Reynolds number ($R_e = \frac{2rv}{\nu}$) that follows during the toss [44]. A range of changes in the Reynolds number is wide because of variations in the coin velocity: $R_e \ll 1$ in the initial stage of its motion (during its fall with a zero initial velocity), $R_e \cong 10^4$ at the velocity of the mass center $v = 10$ m/s and the coin radius $r = 0.01$ m.

For detailed information on the aerodynamics and fluid mechanics pertinent to this section, see [42,47,66,69].

A cylindrical model of the coin with a base radius r and a height h, performing a general motion, is subject to analysis. On the basis of kinematic relations for a rigid body, a distribution of velocities on outer surfaces of the cylinder is determined. It has been assumed that the air resistance occurs only on this part of the cylinder surface on which the velocity vectors of its points have a sense compliant with the normal vector to this surface and directed outwards from the body. The air resistance force vector $\mathbf{f}_r$ is determined on the base as a sum of resistance forces on both the cylinder base planes ($\mathbf{f}_1$ *i* $\mathbf{f}_2$) and resistance forces on the lateral surface ($\mathbf{f}_3$):

$$\mathbf{f}_r = \mathbf{f}_1 + \mathbf{f}_2 + \mathbf{f}_3. \tag{49}$$

The vector $\mathbf{f}_1$ denotes the resistance forces occurring on one plane of the coin ($\zeta = -\frac{h}{2}$), whereas $\mathbf{f}_2$ stands for the resistance forces on the second plane ($\zeta = -\frac{h}{2}$). Each of the vectors $\mathbf{f}_1$, $\mathbf{f}_2$ and $\mathbf{f}_3$ is treated as a sum of two components originating from tangential (parallel) and normal (perpendicular) forces to the body surface. This results in the necessity of using various air resistance coefficients λ_τ for the forces $\mathbf{f}_{i\tau}$ (of the tangential direction (air friction forces)) and λ_n for the forces $\mathbf{f}_{in}$ in the normal direction (air pressure forces). Hence:

$$\mathbf{f}_i = \mathbf{f}_{i\tau} + \mathbf{f}_{in}, \quad (i = 1, 2, 3), \tag{50}$$

where $\mathbf{f}_{1\tau}$ and $\mathbf{f}_{2\tau}$ are determined from the relation

$$\mathbf{f}_{i\tau} = -\lambda_\tau \int_0^r \left(\int_0^{2\pi} |\mathbf{v}_{A_i\tau}|^b \, \mathbf{v}_{A_i\tau} \, \rho \mathrm{d}\theta \right) \mathrm{d}\rho, \quad (i = 1, 2), \tag{51}$$

$$\mathbf{f}_{in} = -\lambda_n \int_0^r \left(\int_0^{2\pi} |\mathbf{v}_{A_in}|^b \, \mathbf{v}_{A_in} \, s_i \, \rho \mathrm{d}\theta \right) \mathrm{d}\rho, \quad (i = 1, 2), \tag{52}$$

and $\mathbf{f}_{1n}$ and $\mathbf{f}_{2n}$ are defined by:

$$\mathbf{f}_{3\tau} = -\lambda_\tau \int_{-h/2}^{h/2} \left(\int_0^{2\pi} |\mathbf{v}_{A_3\tau}|^b \, \mathbf{v}_{A_3\tau} r \mathrm{d}\theta \right) \mathrm{d}z, \tag{53}$$

$$\mathbf{f}_{3n} = -\lambda_n \int_{-h/2}^{h/2} \left(\int_0^{2\pi} |\mathbf{v}_{A_3n}|^b \, \mathbf{v}_{A_3n} s_3 \, r \mathrm{d}\theta \right) \mathrm{d}z. \tag{54}$$

The symbols used in formulae (51)–(54) denote, respectively: r radius of the coin, $\mathbf{v}_{A_i\tau}$ vector comprising the velocity components tangential to the surface on which the point A_i is situated, and $\mathbf{v}_{A_in}$ vector of velocity components perpendicular to this surface, $|\mathbf{v}_{A_i\tau}|$ and $|\mathbf{v}_{A_in}|$ refer to the values of velocity vectors, and b is a real number that belongs to the range $\langle 0, 1\rangle$ (for $b = 0$, the air resistance is linearly dependent on velocity, whereas for $b = 1$, resistance depends on the square of velocity). The functions s_i that occur in formula (52) are described by the following relation:

$$s_i = \frac{1}{2} \operatorname{sgn}(\mathbf{v}_{A_in}^{\mathrm{T}} \boldsymbol{\eta}_i^o) \left(1 + \operatorname{sgn}(\mathbf{v}_{A_in}^{\mathrm{T}} \boldsymbol{\eta}_i^o)\right), \quad (i = 1, 2, 3), \tag{55}$$

where $\boldsymbol{\eta}_i^o$ are unit vectors, normal to the coin surfaces under consideration, directed outwards from the coin (Fig. 13). The vectors $\boldsymbol{\eta}_i^o$ in the *xyz* frame are defined as:

$$\boldsymbol{\eta}_i^o = \mathbf{R}\boldsymbol{\eta}_i, \quad (i = 1, 2, 3), \tag{56}$$

where

$$\boldsymbol{\eta}_1 = \begin{bmatrix} 0 \\ 0 \\ 1 \end{bmatrix}, \qquad \boldsymbol{\eta}_2 = \begin{bmatrix} 0 \\ 0 \\ -1 \end{bmatrix}, \qquad \boldsymbol{\eta}_3 = \begin{bmatrix} \cos\theta \\ \sin\theta \\ 0 \end{bmatrix}. \tag{57}$$

The functions s_i allow for the determination of regions in which the air resistance components normal to the surface act. It has been assumed that normal components of resistance forces do not occur in these regions where the velocity vector of points situated on the surface is directed inwards the body. The air resistance forces perpendicular to the body surface occur in these body points in which the following condition is satisfied:

$$\mathbf{v}_{A_i n}^{\mathrm{T}} \boldsymbol{\eta}_i^o > 0, \quad (i = 1, 2, 3). \tag{58}$$

The effect of application of the functions s_i is illustrated in Fig. 14.

(i) The velocity fields on the coin surfaces.

The symbol $\mathbf{v}_{A_1}$ denotes a column matrix that includes the coordinates of the velocity vector of the point A_1, that is to say, of an arbitrary point situated on the plane $\zeta = \frac{h}{2}$ (Fig. 13). The components of this vector along the normal direction to the surface are represented by the matrix vector $\mathbf{v}_{A_1 n}$, whereas $\mathbf{v}_{A_1 \tau}$ includes the velocity components of the tangential direction to the surface point A_1 is situated on. The tangential and normal components are determined from the relationship:

$$\mathbf{v}_{A_1 n} = \mathbf{R}\mathbf{H}_1\mathbf{R}^{\mathrm{T}}\mathbf{v}_{A_1}, \qquad \mathbf{v}_{A_1 \tau} = \mathbf{v}_{A_1} - \mathbf{v}_{A_1 n}, \tag{59}$$

where

$$\begin{aligned} &\mathbf{v}_{A_1} = \mathbf{v}_B + \boldsymbol{\Omega}\mathbf{r}_{BA_1}, \qquad \mathbf{v}_B = \mathbf{v}_C + \boldsymbol{\Omega}\mathbf{r}_{CB}, \qquad \mathbf{v}_C = [\ \dot{x} \quad \dot{y} \quad \dot{z}\ ]^{\mathrm{T}}, \\ &\mathbf{r}_{BA_1} = \mathbf{R}\boldsymbol{\rho}_1, \qquad \mathbf{r}_{CB} = -\mathbf{R}\boldsymbol{\rho}_{BC}, \\ &\boldsymbol{\rho}_1 = \left[\rho\cos\theta \quad \rho\sin\theta \quad \frac{h}{2}\right]^{\mathrm{T}}, \qquad \boldsymbol{\rho}_{BC} = [\ \xi_C \quad \eta_C \quad \zeta_C\ ]^{\mathrm{T}}, \end{aligned} \tag{60}$$

where $\mathbf{R}$ is a transformation matrix of the coordinates from the frame $\xi\eta\zeta$ into the frame xyz, and $\mathbf{H}_1$ is a zero-one matrix in the form:

$$\mathbf{H}_1 = \begin{bmatrix} 0 & 0 & 0 \\ 0 & 0 & 0 \\ 0 & 0 & 1 \end{bmatrix}. \tag{61}$$

To avoid misunderstanding, let us add that the vectors $\mathbf{v}_{A_1}, \mathbf{v}_B, \mathbf{v}_C, \mathbf{r}_{BA_1}, \mathbf{r}_{CB}, \mathbf{v}_{A_1 n}, \mathbf{v}_{A_1 \tau}$ are defined by the coordinates in the xyz frame, the matrix $\boldsymbol{\Omega}$ is defined in the xyz frame, and the vectors $\boldsymbol{\rho}_1, \boldsymbol{\rho}_{BC}$ are determined by the coordinates in the moving frame $\xi\eta\zeta$. After the transformations that follow from formulae (59) and (60), the expressions that define the components of velocity of individual points lying on the body surface are obtained.

Similarly as for the plane $\zeta = \frac{h}{2}$, the tangential and normal components of the velocity $\mathbf{v}_{A_2}$ of the point A_2 lying on the plane $\zeta = -\frac{h}{2}$ (Fig. 13) are determined:

$$\begin{aligned} &\mathbf{v}_{A_2 n} = \mathbf{R}\mathbf{H}_1\mathbf{R}^{\mathrm{T}}\mathbf{v}_{A_2}, \qquad \mathbf{v}_{A_2 \tau} = \mathbf{v}_{A_2} - \mathbf{v}_{A_2 n}, \qquad \mathbf{v}_{A_2} = \mathbf{v}_B + \boldsymbol{\Omega}\,\mathbf{r}_{BA_2}, \\ &\mathbf{r}_{BA_2} = \mathbf{R}\boldsymbol{\rho}_2, \qquad \boldsymbol{\rho}_2 = \left[\rho\cos\theta \quad \rho\sin\theta \quad -\frac{h}{2}\right]^{\mathrm{T}}. \end{aligned} \tag{62}$$

The symbols $\mathbf{v}_{A_3 n}, \mathbf{v}_{A_3 \tau}$ denote the components of velocity of the point (A_3) lying on the lateral surface of the cylinder that are determined on the basis of the following relation:

$$\begin{aligned} &\mathbf{v}_{A_3 n} = \mathbf{R}\mathbf{R}_\theta\mathbf{H}_3\mathbf{R}_\theta^{\mathrm{T}}\mathbf{R}^{\mathrm{T}}\mathbf{v}_{A_3}, \qquad \mathbf{v}_{A_3 \tau} = \mathbf{v}_{A_3} - \mathbf{v}_{A_3 n}, \\ &\mathbf{v}_{A_3} = \mathbf{v}_B + \boldsymbol{\Omega}\,\mathbf{r}_{BA_3}, \qquad \mathbf{r}_{BA_3} = \mathbf{R}\boldsymbol{\rho}_3, \end{aligned} \tag{63}$$

where $\boldsymbol{\rho}_3$ is a vector that defines the position of this point in the frame $\xi\eta\zeta$:

$$\boldsymbol{\rho}_3 = [\ r\cos\theta \quad r\sin\theta \quad z\ ]^{\mathrm{T}}, \tag{64}$$

and the matrix $\mathbf{H}_3$ has the form as follows:

$$\mathbf{H}_3 = \begin{bmatrix} 1 & 0 & 0 \\ 0 & 0 & 0 \\ 0 & 0 & 0 \end{bmatrix}. \tag{65}$$

Some sample results of the calculations of velocity of points lying on the coin surfaces and the effect of application of the functions s_1, s_2 and s_3 are presented in Fig. 14. The employment of these functions in the calculation procedures allows for the determination of the regions where the components of resistance forces normal to each surface act. The components

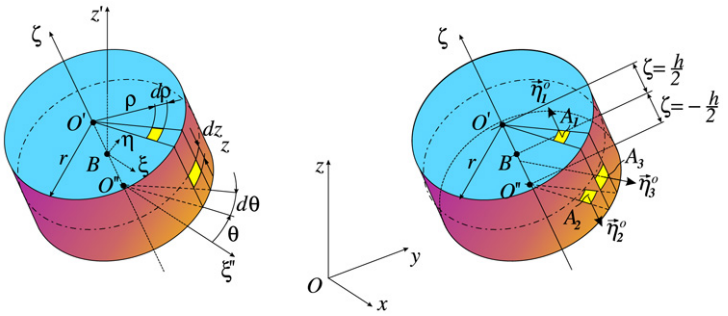

Fig. 13. Quantities used to determine of air resistance forces $\mathbf{f}_1$, $\mathbf{f}_2$ and $\mathbf{f}_3$ (unit vectors of coin planes: $\boldsymbol{\eta}_1^o$, $\boldsymbol{\eta}_2^o$ and cylindrical outer surface $\boldsymbol{\eta}_3^o$).

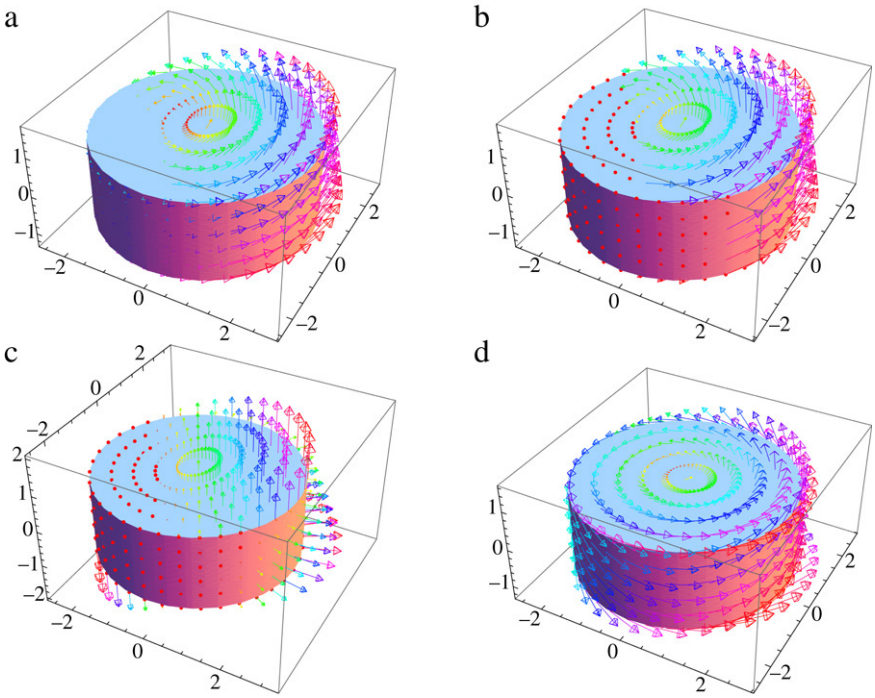

Fig. 14. Velocity vectors of points lying on the coin surfaces: (a) total velocities, (b) velocities with senses directed outwards from the body, (c) normal components with senses directed outwards from the body, (d) tangential components of total velocities.

of air resistance forces tangential to the body surfaces are determined on the whole outer surface of the body. The normal components of resistance forces occur in those regions only where the velocity vector of points lying on the surface is directed outwards from the body (in Fig. 14b and c, the velocity vectors with senses directed inwards the body are shown as points).

(ii) Air resistance forces.

The distribution of air resistance forces corresponds to the velocity distributions of points situated on outer surfaces of the coin. On the assumption that the resistance forces are proportional to velocity (that is to say, after the substitution of $b = 1$ in the formulae describing resistance forces), the distribution of forces normal to individual coin surfaces is such as in Fig. 14c, and the distribution of tangential forces complies with Fig. 14d (the senses of resistance forces are opposite to the senses of the velocity vectors). On the basis of formulae (51) and (52), the resultant of the resistance forces acting on the first coin surface (including the point A_1 (Fig. 13)) is described as:

$$\mathbf{f}_1 = -\lambda_n \int_0^r \left(\int_0^{2\pi} |\mathbf{v}_{A_1 n}|^b \mathbf{v}_{A_1 n} s_1 \rho \mathrm{d}\theta \right) \mathrm{d}\rho - \lambda_\tau \int_0^r \left(\int_0^{2\pi} |\mathbf{v}_{A_1 \tau}|^b \mathbf{v}_{A_1 \tau} \rho \mathrm{d}\theta \right) \mathrm{d}\rho. \tag{66}$$

As has been mentioned before, the function s_1 allows for a selection of regions in which the resistance forces perpendicular to the body surface occur and it is given by the formula:

$$s_1 = \frac{1}{2} \operatorname{sgn}(\mathbf{v}_{A_1 n}^{\mathrm{T}} \boldsymbol{\eta}_1^o) \left(1 + \operatorname{sgn}(\mathbf{v}_{A_1 n}^{\mathrm{T}} \boldsymbol{\eta}_1^o)\right). \tag{67}$$

In a similar way, the resistance forces occurring on the second surface ($\zeta = -\frac{h}{2}$), where the point A_2 is situated (Fig. 13), are determined:

$$\mathbf{f}_2 = -\lambda_n \int_0^r \left(\int_0^{2\pi} |\mathbf{v}_{A_2 n}|^b \mathbf{v}_{A_2 n}\, s_2 \rho \mathrm{d}\theta \right) \mathrm{d}\rho - \lambda_\tau \int_0^r \left(\int_0^{2\pi} |\mathbf{v}_{A_2 \tau}|^b \mathbf{v}_{A_2 \tau} \rho \mathrm{d}\theta \right) \mathrm{d}\rho, \tag{68}$$

where the function s_2 is given by:

$$s_2 = \frac{1}{2} \operatorname{sgn}(\mathbf{v}_{A_2 n}^{\mathrm{T}} \boldsymbol{\eta}_2^o) \left(1 + \operatorname{sgn}(\mathbf{v}_{A_2 n}^{\mathrm{T}} \boldsymbol{\eta}_2^o)\right), \tag{69}$$

where $\boldsymbol{\eta}_2^o$ is a unit vector, normal to the coin surface ($\zeta = -\frac{h}{2}$) and directed outwards from the coin (Fig. 13). The air resistance force ($\mathbf{f}_3$) arising on the lateral side of the cylinder is determined as:

$$\mathbf{f}_3 = -\lambda_n \int_{-h/2}^{h/2} \left(\int_0^{2\pi} |\mathbf{v}_{A_3 n}|^b\, \mathbf{v}_{A_3 n}\, s_3, r \mathrm{d}\theta \right) \mathrm{d}z - \lambda_\tau \int_{-h/2}^{h/2} \left(\int_0^{2\pi} |\mathbf{v}_{A_3 \tau}|^b\, \mathbf{v}_{A_3 \tau}\, r\, \mathrm{d}\theta \right) \mathrm{d}z. \tag{70}$$

Function s_3 takes the form

$$s_3 = \frac{1}{2} \operatorname{sgn}(\mathbf{v}_{A_3 n}^{\mathrm{T}} \boldsymbol{\eta}_3^o) \left(1 + \operatorname{sgn}(\mathbf{v}_{A_3 n}^{\mathrm{T}} \boldsymbol{\eta}_3^o)\right), \tag{71}$$

where $\boldsymbol{\eta}_3^o$ is a unit vector, normal to the cylindrical surface of the coin and directed outwards from the coin.

The distribution of the air resistance forces corresponds to the velocity distributions of points situated on outer surfaces of the coin. On the assumption that the resistance forces are proportional to velocity (that is to say, after the substitution of $b = 1$ in the formulae describing the resistance forces), the distribution of forces normal to individual coin surfaces is such as in Fig. 14c, and the distribution of tangential forces complies with Fig. 14d (the senses of resistance forces are opposite to the senses of velocity vectors). The resultant vectors of tangential forces to each surface can be presented in an explicit (analytical) form.

The resultant vector of the resistance forces $\mathbf{f}_{1n}$, normal to the plane $\zeta = \frac{h}{2}$, is determined on the basis of (66) as $\mathbf{f}_{1n} = -\lambda_n \int_0^r \left(\int_0^{2\pi} |\mathbf{v}_{A_1 n}|^b\, \mathbf{v}_{A_1 n}\, s_1 \rho\, \mathrm{d}\varphi \right) \mathrm{d}\rho$. As in the integrated expression, a selection function of the velocity s_1 occurs, the calculations are conducted numerically for the given numerical data. The numerical calculations are carried out for the discrete velocity field of points lying on the body surface. The integration is performed in these regions only where the velocities of the points ($\mathbf{v}_{A_1 n}$) are directed outwards from the body (Fig. 14c).

Similarly, the resultant vectors of the forces $\mathbf{f}_{2n}$, $\mathbf{f}_{3n}$ are determined numerically, and the vectors $\mathbf{f}_{2\tau}$, $\mathbf{f}_{3\tau}$ are determined explicitly.

(iii) Moments of air resistance forces.

After the determination of forces, the moments of these forces with respect to the center of the mass C (or the chosen pole B) should be determined. The total moment of air resistance forces with respect to the point B has been presented as a sum of the moments ($\mathbf{m}_1$ and $\mathbf{m}_2$) originating from resistance forces on both planes of the cylinder base and the moments of resistance forces on the lateral surface ($\mathbf{m}_3$):

$$\mathbf{m}_{rB} = \mathbf{m}_1 + \mathbf{m}_2 + \mathbf{m}_3, \tag{72}$$

where $\mathbf{m}_1$ and $\mathbf{m}_2$are determined from the formula (73) (for $i = 1,\ 2$)

$$\mathbf{m}_i = -\lambda_n \int_0^r \left(\int_0^{2\pi} |\mathbf{v}_{A_i n}|^b\, \mathbf{R}^{\mathrm{T}} \mathbf{R}_{BA_i} \mathbf{v}_{A_i n}\, s_i\, \rho \mathrm{d}\theta \right) \mathrm{d}\rho - \lambda_\tau \int_0^r \left(\int_0^{2\pi} |\mathbf{v}_{A_i \tau}|^b\, \mathbf{R}^{\mathrm{T}} \mathbf{R}_{BA_i} \mathbf{v}_{A_i \tau}\, \rho \mathrm{d}\theta \right) \mathrm{d}\rho, \tag{73}$$

whereas $\mathbf{m}_3$ is expressed by the relation:

$$\mathbf{m}_3 = -\lambda_n \int_{-h/2}^{h/2} \left(\int_0^{2\pi} |\mathbf{v}_{A_3 n}|^b\, \mathbf{R}^{\mathrm{T}} \mathbf{R}_{BA_3} \mathbf{v}_{A_3 n}\, s_3\, r \mathrm{d}\theta \right) \mathrm{d}z - \lambda_\tau \int_{-h/2}^{h/2} \left(\int_0^{2\pi} |\mathbf{v}_{A_3 \tau}|^b\, \mathbf{R}^{\mathrm{T}} \mathbf{R}_{BA_3} \mathbf{v}_{A_3 \tau}\, r \mathrm{d}\theta \right) \mathrm{d}z, \tag{74}$$

where $\mathbf{R}_{BA_1}$, $\mathbf{R}_{BA_2}$, and $\mathbf{R}_{BA_3}$ in formulae (73) and (74) denote antisymmetrical matrices including the components of the vectors $\mathbf{r}_{BA_1}$ (60), $\mathbf{r}_{BA_2}$ (62) and $\mathbf{r}_{BA_3}$ (63), respectively, that can be expressed symbolically as $\mathbf{R}_{BA_1} = \tilde{\mathbf{r}}_{BA_1}$, $\mathbf{R}_{BA_2} = \tilde{\mathbf{r}}_{BA_2}$, $\mathbf{R}_{BA_3} = \tilde{\mathbf{r}}_{BA_3}$.

Only the tangent components of resultant moment of air resistance forces $\mathbf{m}_{rB}$ are determined explicitly. The normal components are calculated numerically after the discretization of actual velocity field on the coin body.

(iv) Simplified model of coin–air interaction.

If the thickness of the coin h is negligible in comparison to its radius r, then it can be assumed that $h \to 0$ (or $h = 0$) in the computational model. Thus, the formulae generated in the previous subsection can be employed after the substitution of $h = 0$.

In this subsection, we show how the formulae that describe air resistance for a simplified 2D model of the coin can be derived from the general relationships. In this way the relations that define not only the resultant of the air resistance forces

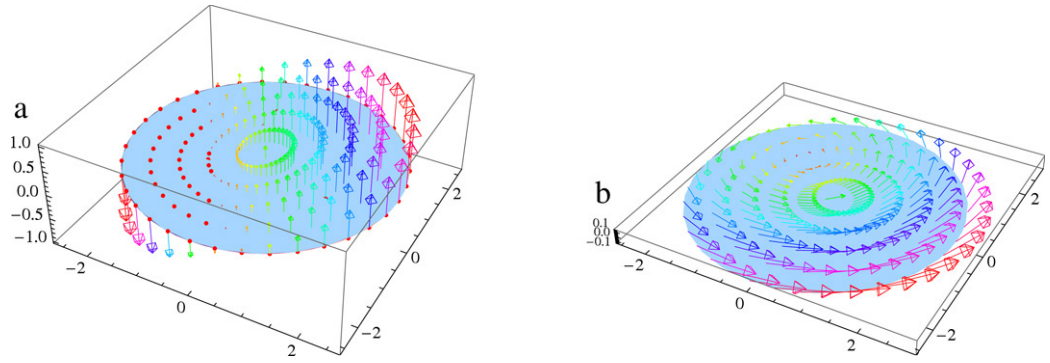

Fig. 15. Velocity vectors of points situated on the surfaces of the 2D coin model: (a) normal velocity components with senses outwards from the body, (b) tangential components of total velocities.

tangential to the coin surface, but also the resultant of normal forces can be determined explicitly. For a thin coin ($h = 0$), the velocities of points situated on both planes are identical:

$$\mathbf{v}_{A_1} = \mathbf{v}_{A_2}, \qquad \mathbf{v}_{A_1\tau} = \mathbf{v}_{A_2\tau}, \qquad \mathbf{v}_{A_1 n} = \mathbf{v}_{A_2 n}. \tag{75}$$

After the calculations in which the general relations (59) and (60) have been used, the normal components of velocity (for $h = 0$ and $\zeta_C = 0$) are obtained in the explicit form. The velocity vectors of points situated on both planes of the 2D coin model have been depicted in Fig. 15.

(vi) Resistance forces for thin coin.

While determining a sum of normal components of the resistance forces ($\mathbf{f}_{1n} + \mathbf{f}_{2n}$), acting on the planes at both sides of the coin, we obtain on the basis of (52):

$$\mathbf{f}_{1n} + \mathbf{f}_{2n} = -\lambda_{n1} \int_0^r \left(\int_0^{2\pi} |\mathbf{v}_{A_1 n}|^b \mathbf{v}_{A_1 n}\, s_1\, \rho \mathrm{d}\theta \right) \mathrm{d}\rho - \lambda_{n2} \int_0^r \left(\int_0^{2\pi} |\mathbf{v}_{A_2 n}|^b \mathbf{v}_{A_2 n}\, s_2\, \rho \mathrm{d}\theta \right) \mathrm{d}\rho. \tag{76}$$

On the assumption that the coefficients λ_{n1} and λ_{n2} are identical ($\lambda_{n1} = \lambda_{n2} = \lambda_n$), relation (76) can be expressed as:

$$\mathbf{f}_{1n} + \mathbf{f}_{2n} = -\lambda_n \int_0^r \left(\int_0^{2\pi} |\mathbf{v}_{A_1 n}|^b \mathbf{v}_{A_1 n}\, (s_1 + s_2)\, \rho \mathrm{d}\theta \right) \mathrm{d}\rho. \tag{77}$$

From the properties of the functions s_1 (67) and s_2 (69), it results that in the case under consideration ($\mathbf{v}_{A_1 n} = \mathbf{v}_{A_2 n}$ and $\boldsymbol{\eta}_1^o = -\boldsymbol{\eta}_2^o$):

$$s_1 + s_2 = \frac{1}{2} \operatorname{sgn}(\mathbf{v}_{A_1 n}^{\mathrm{T}} \boldsymbol{\eta}_1^o) \left(1 + \operatorname{sgn}(\mathbf{v}_{A_1 n}^{\mathrm{T}} \boldsymbol{\eta}_1^o)\right) + \tag{78}$$

$$+ \frac{1}{2} \operatorname{sgn}(\mathbf{v}_{A_1 n}^{\mathrm{T}} (-\boldsymbol{\eta}_1^o)) \left(1 + \operatorname{sgn}(\mathbf{v}_{A_1 n}^{\mathrm{T}} (-\boldsymbol{\eta}_1^o))\right) = 1. \tag{79}$$

Thus, the resultant of the resistance forces with normal directions to the coin surface ($\mathbf{f}_{1n} + \mathbf{f}_{2n}$) can be expressed by the formula:

$$\mathbf{f}_{1n} + \mathbf{f}_{2n} = -\lambda_n \int_0^r \left(\int_0^{2\pi} |\mathbf{v}_{A_1 n}|^b\, \mathbf{v}_{A_1 n}\, \rho \mathrm{d}\theta \right) \mathrm{d}\rho. \tag{80}$$

If it is additionally assumed that for the thin coin ($h = 0$), the air forces acting on the coin cylindrical surface equal zero ($\mathbf{f}_{3n} = \mathbf{0}$ and $\mathbf{f}_{3\tau} = \mathbf{0}$), one gets:

$$\mathbf{f}_n = \mathbf{f}_{1n} + \mathbf{f}_{2n} + \mathbf{f}_{3n} = -\lambda_n \int_0^r \left(\int_0^{2\pi} |\mathbf{v}_{A_1 n}|^b\, \mathbf{v}_{A_1 n} \rho \mathrm{d}\theta \right) \mathrm{d}\rho. \tag{81}$$

The determination of the resultant of the forces tangential to the coin surface ($\mathbf{f}_\tau = \mathbf{f}_{1\tau} + \mathbf{f}_{2\tau} + \mathbf{f}_{3\tau}$), defined by (51), on the assumption that $\mathbf{f}_{3\tau} = \mathbf{0}$, $\mathbf{v}_{A_1\tau} = \mathbf{v}_{A_2\tau}$ and $\lambda_{\tau 1} = \lambda_{\tau 2} = \lambda_\tau$, leads to:

$$\mathbf{f}_\tau = \mathbf{f}_{1\tau} + \mathbf{f}_{2\tau} + \mathbf{f}_{3\tau} = -2\,\lambda_\tau \int_0^r \left(\int_0^{2\pi} |\mathbf{v}_{A_1\tau}|^b\, \mathbf{v}_{A_1\tau}\, \rho \mathrm{d}\theta \right) \mathrm{d}\rho. \tag{82}$$

(vii) Moments of resistance forces for a thin coin.

Similarly, as with the forces, the moments originating from the resistance forces acting on the lateral surface of the coin are neglected ($\mathbf{m}_3 = \mathbf{0}$) in the case of the thin coin. While determining a sum of the moments of normal components of

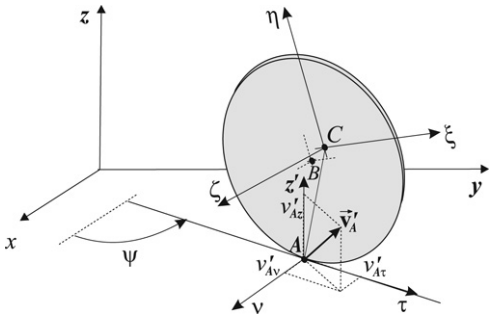

Fig. 16. Velocity vector $\vec{\mathbf{v}}'_A$ of the point A after the collision and its scalar components $v'_{A\tau}, v'_{A\nu}, v'_{Az}$.

resistance forces ($\mathbf{m}_1+\mathbf{m}_2$), acting on the planes on both sides of the coin, on the basis of (73) (for $\mathbf{v}_{A_1} = \mathbf{v}_{A_2}, \lambda_{n1} = \lambda_{n2} = \lambda_n$, $\lambda_{\tau 1} = \lambda_{\tau 2} = \lambda_\tau$), we obtain:

$$\mathbf{m}_{Bn} = \mathbf{m}_{1n} + \mathbf{m}_{2n} = -\lambda_n \int_0^r \left(\int_0^{2\pi} |\mathbf{v}_{A_1 n}|^b \, \mathbf{R}^{\mathrm{T}} \mathbf{R}_{BA_1} \mathbf{v}_{A_1 n} \, \rho \mathrm{d}\theta \right) \mathrm{d}\rho, \tag{83}$$

$$\mathbf{m}_{B\tau} = \mathbf{m}_{1\tau} + \mathbf{m}_{2\tau} = -2\,\lambda_\tau \int_0^r \left(\int_0^{2\pi} |\mathbf{v}_{A_1 \tau}|^b \, \mathbf{R}^{\mathrm{T}} \mathbf{R}_{BA_1} \mathbf{v}_{A_1 \tau} \, \rho \mathrm{d}\theta \right) \mathrm{d}\rho. \tag{84}$$

For the thin coin ($h = 0$), both tangential and normal components of the resistance force moment vector with respect to the point B (and the point C) can be defined explicitly.

4.3. Impacts against the floor

Let us consider that the imperfect coin collides with a floor when the point A on its edge touches the floor as shown in Fig. 16. Assuming Newton's hypothesis one gets

$$-\chi = \frac{v'_{Az}}{v_{Az}}, \tag{85}$$

where χ is the coefficient of restitution, A stands for the coin point which makes contact with the floor at the instant of impact (Fig. 16), v'_{Az} and v_{Az} are projections of the velocity of the point A on the direction (z) normal to the impact surface, before and after the impact, respectively.

The position of the point A in the body embedded frame is described by ξ_A, η_A, ζ_A (point A is located on the coin edge in one of the coin planes). To describe the impacts consider the additional frame with an origin at point A and axis: z' — parallel to the fixed axis z and axes τ, $\ni$ in the ground plane (Fig. 16).

To analyze the phenomena that accompany the impact, Newton's hypothesis, the laws of linear momentum and angular momentum theorems of a body, as well as constraint equations have been employed. These equations – expressed in Euler parameters – have the following form:

– Newton's hypothesis

$$\begin{aligned}
&\left(2e_0{}^2 + 2e_3{}^2 - 1\right)(\omega'_\xi \eta_A - \omega'_\eta \xi_A) + (2e_0 e_1 + 2e_2 e_3)(\omega'_\zeta \xi_A - \omega'_\xi \zeta_A) + (2e_1 e_3 - 2e_0 e_2)(\omega'_\eta \zeta_A - \omega'_\zeta \eta_A) + \dot{z}' \\
&\quad = -\chi \left(\left(2e_0{}^2 + 2e_3{}^2 - 1\right)(\omega_\xi \eta_A - \omega_\eta \xi_A) + (2e_0 e_1 + 2e_2 e_3)(\omega_\zeta \xi_A - \omega_\xi \zeta_A) \right. \\
&\qquad \left. + (2e_1 e_3 - 2e_0 e_2)(\omega_\eta \zeta_A - \omega_\zeta \eta_A) + \dot{z} \right),
\end{aligned} \tag{86}$$

– linear momentum theorem

$$m\dot{x}' - S_x = m\dot{x}, \qquad m\dot{y}' - S_y = m\dot{y}, \qquad m\dot{z}' - S_z = m\dot{z}, \tag{87}$$

– angular momentum theorem

$$\begin{aligned}
&2\zeta_A S_y e_0{}^2 - 2\eta_A S_z e_0{}^2 - 2e_2 \eta_A S_x e_0 - 2e_3 \zeta_A S_x e_0 + 2e_1 \eta_A S_y e_0 + 2e_1 \zeta_A S_z e_0 + J_\xi \omega'_\xi - J_{\xi\eta} \omega'_\eta \\
&\quad - J_{\xi\zeta} \omega'_\zeta - 2e_1 e_3 \eta_A S_x + 2e_1 e_2 \zeta_A S_x - 2e_2 e_3 \eta_A S_y + 2e_2{}^2 \zeta_A S_y - \zeta_A S_y - 2e_3{}^2 \eta_A S_z + \eta_A S_z + 2e_2 e_3 \zeta_A S_z \\
&\quad = J_\xi \omega_\xi - J_{\xi\eta} \omega_\eta - J_{\xi\zeta} \omega_\zeta,
\end{aligned} \tag{88}$$

$$\begin{aligned}
&-2\zeta_A S_x e_0{}^2 + 2\xi_A S_z e_0{}^2 + 2e_2 \xi_A S_x e_0 - 2e_1 \xi_A S_y e_0 - 2e_3 \zeta_A S_y e_0 + 2e_2 \zeta_A S_z e_0 - J_{\xi\eta} \omega'_\xi + J_\eta \omega'_\eta - J_{\eta\zeta} \omega'_\zeta \\
&\quad + 2e_1 e_3 \xi_A S_x - 2e_1{}^2 \zeta_A S_x + \zeta_A S_x + 2e_2 e_3 \xi_A S_y - 2e_1 e_2 \zeta_A S_y + 2e_3{}^2 \xi_A S_z - \xi_A S_z - 2e_1 e_3 \zeta_A S_z \\
&\quad = -J_{\xi\eta} \omega_\xi + J_\eta \omega_\eta - J_{\eta\zeta} \omega_\zeta,
\end{aligned} \tag{89}$$

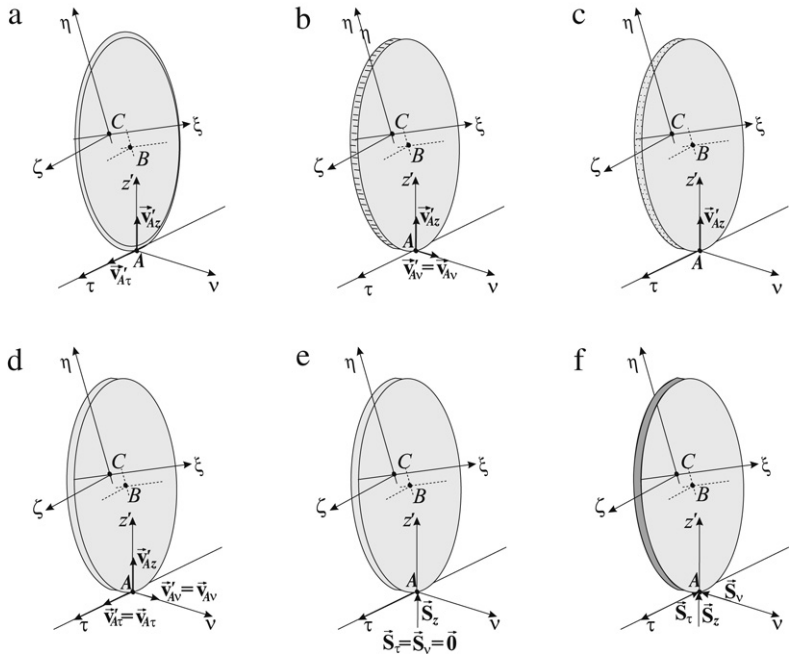

Fig. 17. Coin-surface collision models: (a) the coin with a sharp edge, (b) the knurled coin, (c) the perfectly rough coin, (d) the smooth (frictionless) coin (1), (e) the smooth (frictionless) coin (2), (f) the rough coin with developed friction.

$$
\begin{aligned}
&2\eta_A S_x e_0{}^2 - 2\xi_A S_y e_0{}^2 + 2e_3\xi_A S_x e_0 + 2e_3\eta_A S_y e_0 - 2e_1\xi_A S_z e_0 - 2e_2\eta_A S_z e_0 - J_{\xi\zeta}\omega'_\xi - J_{\eta\zeta}\omega'_\eta \\
&\quad + J_\zeta\omega'_\zeta - 2e_1e_2\xi_A S_x + 2e_1{}^2\eta_A S_x - \eta_A S_x - 2e_2{}^2\xi_A S_y + \xi_A S_y + 2e_1e_2\eta_A S_y - 2e_2e_3\xi_A S_z + 2e_1e_3\eta_A S_z \\
&\quad = -J_{\xi\zeta}\omega_\xi - J_{\eta\zeta}\omega_\eta + J_\zeta\omega_\zeta . \qquad (90)
\end{aligned}
$$

S_x, S_y, S_z are the components of the impulse of base reaction ($\vec{\mathbf{S}}$) defined in the fixed frame of coordinates (x, y, z); $\omega_\xi, \omega_\eta, \omega_\zeta$ denote the components of the angular velocity in the moving frame of reference ξ, η, ζ. There are nine unknowns in Eqs. (86)–(90). These equations are ordered in such a way that the unknown quantities $(\dot{x}', \dot{y}', \dot{z}', \omega'_\xi, \omega'_\eta, \omega'_\zeta, S_x, S_y, S_z)$ are on the left-hand side.

To obtain two additional equations we have to consider the model of the contact between the coin and the horizontal plane surface (ground, floor). According to Nejmark and Fufaev [53] several different models of collision effect can be considered as shown in Fig. 17. The individual cases differ as far as the values of the components of the velocity vector of the contact point (A) of the coin with the surface along the tangential direction (before the impact ($v_{A\tau}$) and after the impact ($v'_{A\tau}$)) and along the normal direction ($v_{A\nu}$ and $v'_{A\nu}$) or the impulse of the ground reaction ($\vec{\mathbf{S}}_{\tau\nu}$) are concerned, namely:

(a) the coin with a sharp edge $v'_{Az} = -\chi v_{Az}$, $v'_{A\nu} = 0$, $v'_{A\tau} = v_{A\tau}$,
(b) the knurled coin $v'_{Az} = -\chi v_{Az}$, $v'_{A\nu} = v_{A\nu}$, $v'_{A\tau} = 0$,
(c) the perfectly rough coin $v'_{Az} = -\chi v_{Az}$, $v'_{A\nu} = 0$, $v'_{A\tau} = 0$,
(d) the smooth-frictionless coin (1) $v'_{Az} = -\chi v_{Az}$, $v'_{A\nu} = v_{A\nu}$, $v'_{A\tau} = v_{A\tau}$,
(e) the smooth-frictionless coin (2) $v'_{Az} = -\chi v_{Az}$, $\vec{\mathbf{S}}_{\tau\nu} = \vec{\mathbf{0}}$,
(f) the rough coin with developed friction $v'_{Az} = -\chi v_{Az}$, $\vec{\mathbf{S}}_{\tau\nu} = -\mu S_z \frac{\vec{\mathbf{v}}_{A\tau\nu}}{v_{A\tau\nu}}$.

$\vec{\mathbf{S}}_{\tau\nu}$ is the component on the floor reaction impulse located in the floor plane and μ the coefficient of dry friction between the coin and the floor.

In the case of the rough coin conditions: $v'_{A\nu} = 0$, $v'_{A\tau} = 0$ imply the following constraint equations:

$$
\begin{aligned}
&(2e_0e_2 + 2e_1e_3)(\omega'_\xi\eta_A - \omega'_\eta\xi_A) + (2e_1e_2 - 2e_0e_3)(\omega'_\zeta\xi_A - \omega'_\xi\zeta_A) \\
&\quad + \left(2e_0{}^2 + 2e_1{}^2 - 1\right)(\omega'_\eta\zeta_A - \omega'_\zeta\eta_A) + \dot{x}' = 0, \qquad (91) \\
&(2e_2e_3 - 2e_0e_1)(\omega'_\xi\eta_A - \omega'_\eta\xi_A) + \left(2e_0{}^2 + 2e_2{}^2 - 1\right)(\omega'_\zeta\xi_A - \omega'_\xi\zeta_A) \\
&\quad + (2e_1e_2 + 2e_0e_3)(\omega'_\eta\zeta_A - \omega'_\zeta\eta_A) + \dot{y}' = 0. \qquad (92)
\end{aligned}
$$

Solving Eqs. (86)–(92) one gets the components of velocity of the center of the coin mass after the collision $\dot{x}', \dot{y}', \dot{z}'$ and the components of the coin angular velocity $\omega'_\xi, \omega'_\eta, \omega'_\zeta$. Additionally, the components of the impulse reaction S_x, S_y, S_z are calculated.

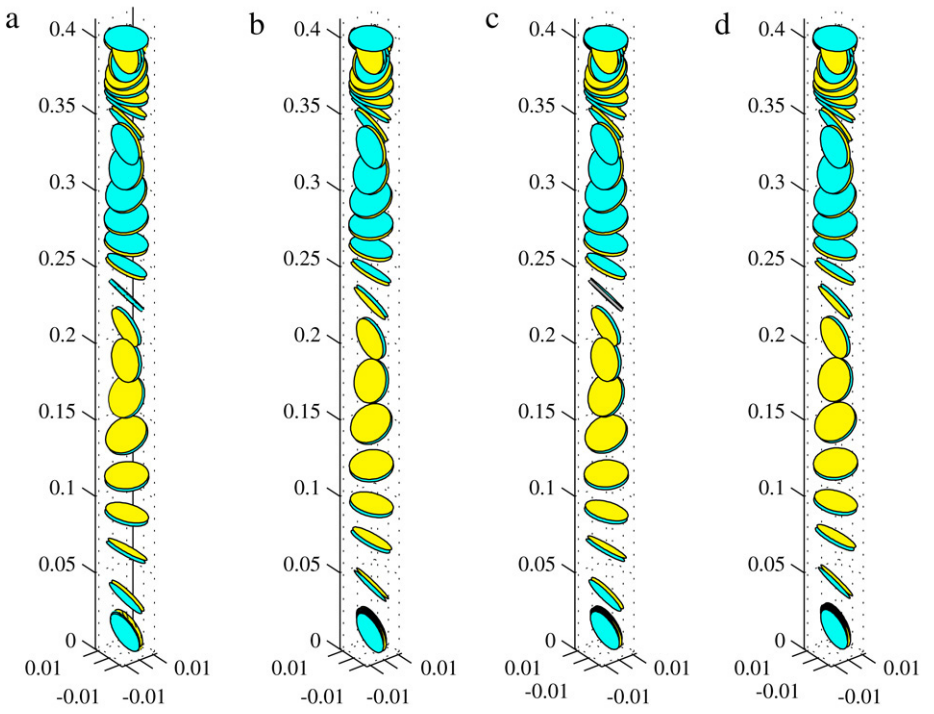

Fig. 18. Coin motion simulation results: (a) 3D imperfect coin model, (b) 3D ideal coin model, (c) 2D imperfect coin model, (d) 2D ideal coin model.

In the case of a smooth ideal coin equations (86)–(90) can be simplified as $J_{\xi\eta} = J_{\xi\zeta} = J_{\eta\zeta} = 0$ to the following form:

$$\begin{aligned}&\left(2{e_0}^2 + 2{e_3}^2 - 1\right)(\omega'_\xi \eta_A - \omega'_\eta \xi_A) + (2e_0e_1 + 2e_2e_3)(\omega'_\zeta \xi_A - \omega'_\xi \zeta_A) + (2e_1e_3 - 2e_0e_2)(\omega'_\eta \zeta_A - \omega'_\zeta \eta_A) + \dot{z}' \\ &\quad = -\chi\left(\left(2{e_0}^2 + 2{e_3}^2 - 1\right)(\omega_\xi \eta_A - \omega_\eta \xi_A) + (2e_0e_1 + 2e_2e_3)(\omega_\zeta \xi_A - \omega_\xi \zeta_A)\right. \\ &\qquad \left. + (2e_1e_3 - 2e_0e_2)(\omega_\eta \zeta_A - \omega_\zeta \eta_A) + \dot{z}\right), \end{aligned} \tag{93}$$

$$m(\dot{x}' - \dot{x}) = 0, \qquad m(\dot{y}' - \dot{y}) = 0, \qquad m(\dot{z}' - \dot{z}) = S_z, \tag{94}$$

$$J_\xi \omega'_\xi + \left(-2\eta_A {e_0}^2 + 2e_1\zeta_A e_0 - 2{e_3}^2\eta_A + \eta_A + 2e_2e_3\zeta_A\right) S_z = J_\xi \omega_\xi, \tag{95}$$

$$J_\eta \omega'_\eta + \left(2\xi_A {e_0}^2 + 2e_2\zeta_A e_0 + 2{e_3}^2\xi_A - \xi_A - 2e_1e_3\zeta_A\right) S_z = J_\eta \omega_\eta, \tag{96}$$

$$J_\zeta \omega'_\zeta \left(-2e_1\xi_A e_0 - 2e_2\eta_A e_0 - 2e_2e_3\xi_A + 2e_1e_3\eta_A\right) S_z = J_\zeta \omega_\zeta. \tag{97}$$

5. Results and discussion

5.1. The comparison of different coin models

In our numerical calculations we consider the following coin data: $m = 2$ g, $r = 1.25$ cm, $h = 0.2$ cm (former Polish 1 PLN coin made of a light aluminum based alloy) and $\xi_C = -0.1$ cm, $\eta_C = -0.1$ cm, $\zeta_C = -0.02$ cm. For numerical simulations we used a standard Mathematica package [48,68].

Results of simulations of the coin motion during the free fall for neglected air resistance have been shown in Fig. 18(a–d) (and Fig. 19(a–d)). Fig. 18(a, b) shows a simulation of the motion of the 3D imperfect (Fig. 18(a)) and ideal (Fig. 18(b)) coin models (Eqs. (29)–(36) respectively). Fig. 18(c, d) presents results for a 2D model of imperfect (Fig. 18(c)) and ideal (Fig. 18(d)) thin coins (Eqs. (37)–(39)).

A comparison of different coin models in the presence of air resistance is shown in Fig. 20 where the trajectories calculated with different models are presented in green (3D imperfect coin), navy blue (3D ideal coin), blue (2D imperfect coin) and red (2D ideal coin).

The effect of air resistance is better visible in the exemplary calculations conducted for an ideal coin ($\xi_C = 0$, $\zeta_C = 0$) with negligible thickness ($h = 0$) and with the assumption that the axes $\xi\eta\zeta$ are the main axes of inertia. The data assumed in the calculations are the same scaled parameters as in [67,49] (i.e., $r = 1$ m, $m = 1$ kg, $g = 1$ m/s^2). The coin falls from the assumed height z_0 with a zero initial velocity of the mass center and the assumed initial angular velocity $\omega_{\xi 0} = \dot{\vartheta}_0$ ($\omega_\eta = 0$, $\omega_\zeta = 0$). The coin dynamics can be described assuming the plane motion in the yz plane (the angles of spin and precession

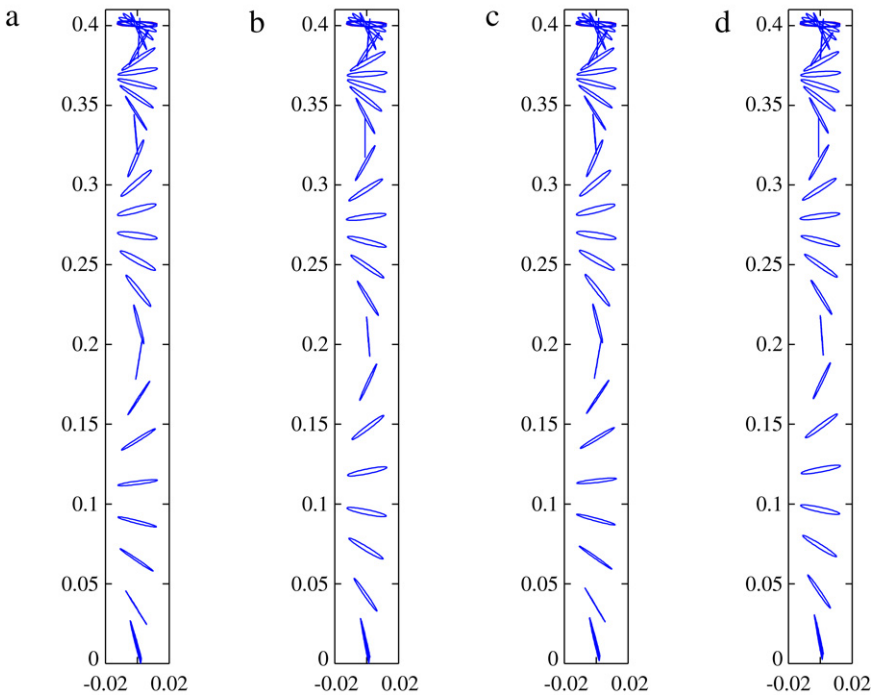

Fig. 19. Coin motion simulation results (projection to the *xz* plane): (a) 3D imperfect coin model, (b) 3D ideal coin model, (c) 2D imperfect coin model, (d) 2D ideal coin model.

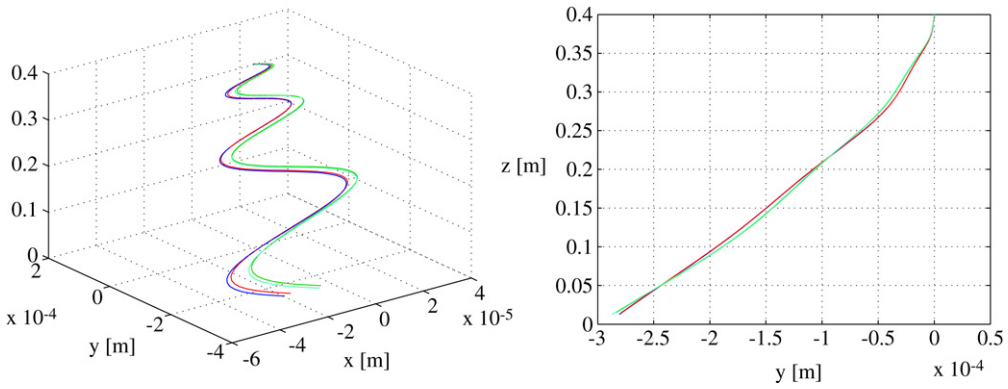

Fig. 20. Free fall coin mass center trajectories for: 3D imperfect coin (green), 3D ideal coin (navy blue), 2D imperfect coin (blue) and 2D ideal coin (red). (For interpretation of the references to colour in this figure legend, the reader is referred to the web version of this article.)

are equal to zero, $\varphi = \psi = 0$). Moreover, it has been assumed that air resistance is linearly dependent on velocity (the case where $b = 0$ is considered). The values of components of resistance forces have been determined from relations (81)–(82). The total moment of resistance forces with respect to the geometrical center (B), for the model of the thin, ideal coin under analysis, has been defined on the basis of (84).

Fig. 21 presents an exemplary diagram showing changes in the velocity (Fig. 21(a)) and acceleration (Fig. 21(b)) of the mass center of the coin, including the air resistance effect, whereas Fig. 22 depicts changes in the rotation angle ϑ (coin inclination angle) and the vertical component of the resistance force f_{rz}. Solid lines represent the cases where air resistance has been neglected whereas the broken lines have been calculated for air resistance characterized by $\lambda_n = 0.3$, $\lambda_\tau = 0$.

It follows from the comparison of individual quantities, including the effect of air resistance and neglecting the effect of these resistance forces, that an influence of resistance can be significant (as in the case of $\lambda = 0.3$). The velocity and acceleration of the mass center are not straight lines – as in the case where resistance is neglected – but they exhibit an oscillating character (similarly as the force f_{rz}). The frequency of these oscillations decreases with a decrease in the coin

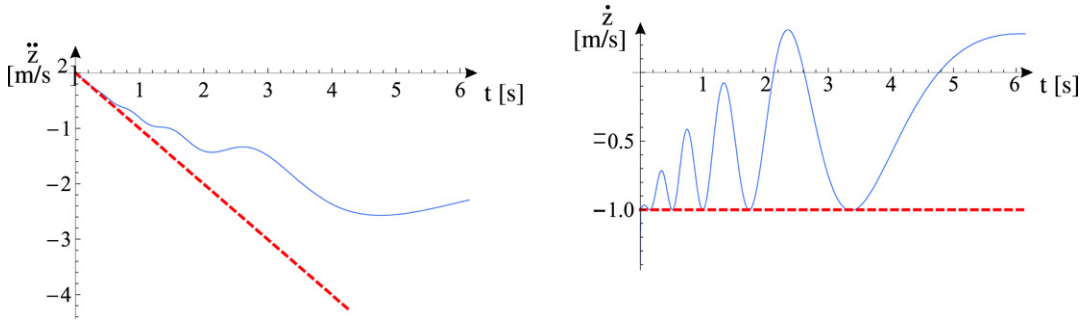

Fig. 21. Time series of the mass center of an ideal coin: $r = 1$ m, $m = 1$ kg, $g = 1$ m/s^2; air resistance characterized by $\lambda_n = 0.3$, $\lambda_\tau = 0$ — solid line, air resistance neglected — dotted line.

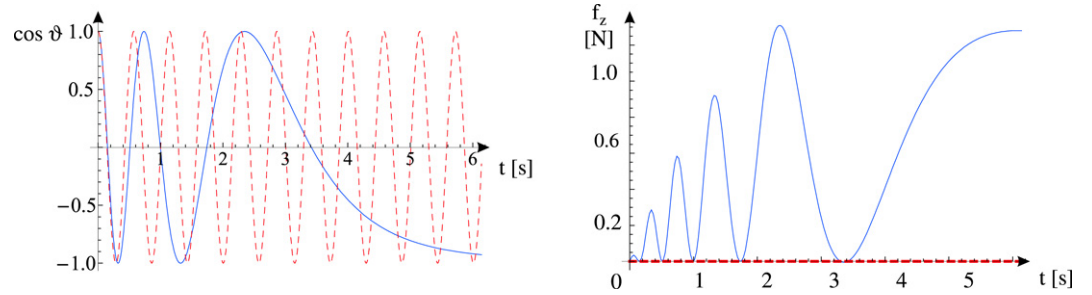

Fig. 22. Time series of cosine ϑ (coin inclination angle) and air resistance vertical component (f_{rz}): $r = 1$ m, $m = 1$ kg, $g = 1$ m/s^2; air resistance characterized by $\lambda_n = 0.3$, $\lambda_\tau = 0$ — solid line, air resistance neglected — dotted line.

angular velocity ($\dot{\vartheta}$). The plot of the function $\cos\vartheta$ points out to the fact that changes in the angle ϑ occur slower and slower, and at the sufficiently long fall time, ϑ attains a constant value.

Generally, air resistance is a potential confounding factor. The air resistance causes the deviation of the trajectory of the mass center from the vertical axis and damps the rotation of the coin. In the case of the real coin, this deviation is small and only if the distance of the free fall is very long (tens of meters) the coin falls like a leaf, fluttering to the floor.

Eqs. (29)–(39) describe the case where the free fall of different coin models are differentiable so that one can calculate transient Lyapunov exponents. By transient Lyapunov exponents we mean values obtained for a finite t not large enough to ensure a satisfactory reduction of fluctuations but small enough to reveal slow trends [65,33,34]. Our calculations show that for sufficiently large t all transient Lyapunov exponents tend to zero, so there is no sensitive dependence on initial conditions during the free fall.

Results for the simulation of the coin bouncing on the floor are shown in Fig. 23. Trajectories calculated from different models are indicated as in Fig. 20. Fig. 24 presents the trajectories of the coin mass center calculated for slightly different initial conditions z_0: $z_0 = 0.40001$ (Fig. 24(a)), $z_0 = 0.40002$ (Fig. 24(b)), $z_0 = 0.40003$ (Fig. 24(c)), $z_0 = 0.40004$ (Fig. 24(d)), $z_0 = 0.40005$ (Fig. 24(e)), $z_0 = 0.40006$ (Fig. 24(f)). The other initial conditions have been fixed to $x_0 = y_0 = 0$, $\dot{x}_0 = \dot{y}_0 = \dot{z}_0 = 0$, $\varphi_0 = \psi_0 = 0$, $\vartheta_0 = 7\pi/180$ rad, $\omega_{\xi 0} = \omega_{\zeta 0} = 0$, $\omega_{\eta 0} = 40.15$ rad/s.

The sequences indicating which face of the coin is up after the successive impact in the simulations shown in Fig. 24 are as follows:

(a) $H \circ HHH \circ HHH \circ HHH \circ T \circ T \circ T \circ HH$ for $z_0 = 0.40001$,
(b) $H \circ HHH \circ HH \circ TT \circ HHH \circ T \circ T \circ T$ for $z_0 = 0.40002$,
(c) $H \circ HHH \circ HHH \circ HH \circ H \circ T \circ T \circ T \circ T \circ T$ for $z_0 = 0.40003$,
(d) $H \circ HHH \circ TTT \circ TTT \circ T \circ H \circ H \circ H \circ H \circ H$ for $z_0 = 0.40004$,
(e) $H \circ HHH \circ HHH \circ TTT \circ HHH \circ H \circ T \circ TT$ for $z_0 = 0.40005$,
(f) $H \circ HHH \circ HHHH \circ TT \circ T \circ HHHHH \circ TT$ for $z_0 = 0.40006$.

Some of the collisions are not visible in the scale of Fig. 24 as they occur in small time intervals. More details are visible at the enlargements shown in Fig. 25.

In the presented examples one can notice that bouncing on the floor introduces a dependence on the initial conditions. This dependence is better visible in Fig. 26. Trajectories of the coin center of mass starting from slightly different initial conditions are shown in different colors. One can notice that in few initial impacts trajectories differ significantly from each other.

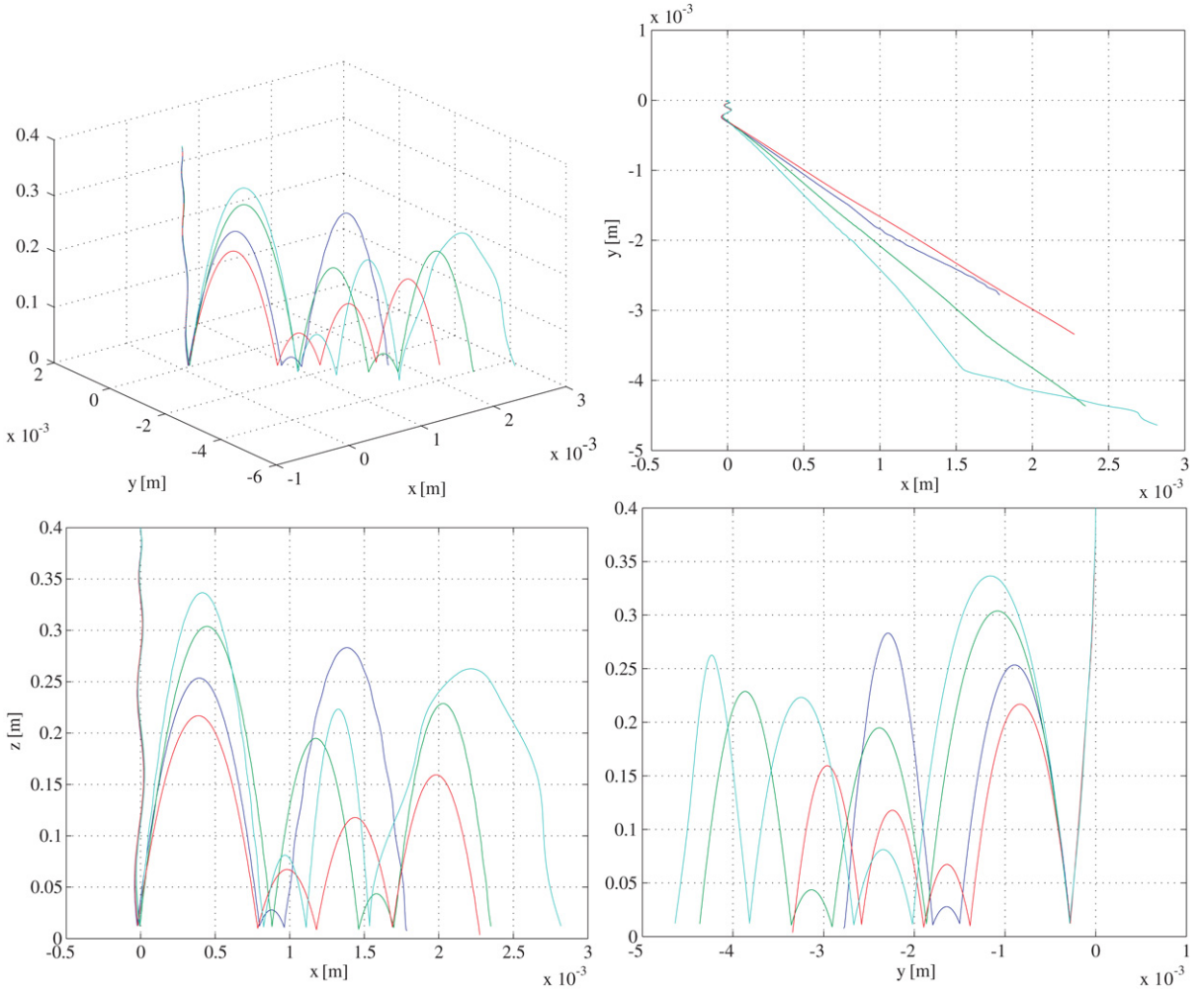

Fig. 23. Coin mass center trajectories after collisions for: 3D imperfect coin (green), 3D ideal coin (navy blue), 2D imperfect coin (blue) and 2D ideal coin (red). (For interpretation of the references to colour in this figure legend, the reader is referred to the web version of this article.)

The dependence on the initial conditions due to impact can lead to unpredictability and chaotic behavior in mechanical systems [29,30]. To quantify the dependence on the initial conditions we introduced the following map. Let $U : [0, 2\pi] \to [0, 2\pi]$ be a map which maps the point ϕ_n on the edge of the coin which hits the floor at the nth impact to the point ϕ_{n_1} which hits the floor at the $(n+1)$th impact. An example of such a map is shown in Fig. 27. The left part of Fig. 27 shows the points on the edge of the coin which collide with the floor at successive collisions. Numbers around the coin edge indicate points of the few initial collisions. The analysis of the time series of points $\phi_1, \phi_2, \ldots,$ shows that the dynamics of U is characterized by transient chaotic behavior as the largest transient Lyapunov exponent is positive (equal to 0.024).

Our simulations reveal that from the point of determining the final outcome (heads or tails) two types of collisions shown in Fig. 28(a–c) are possible. In the first scenario after many soft chattering collisions (occurring in exponentially decreasing time intervals) which orient the coin closer to being perpendicular to the surface the coin finally flips over (Fig. 28(a)). After the nth collision the coin flips over during the free motion before the next $(n+1)$th collision. The second type is characterized by the larger momentum transfer during the collision which allows the coin to flip around during the motion over the floor (Fig. 28(b)). The observation of the side of the coin which is up after a successive collision, allows us to identify both types of collisions (Fig. 28(c)). If the same side (say heads) is up in a number of collisions after which, one observes a flip to another side (say tails), the sequence of soft chattering collisions takes place. When after a single tails side one observes a flip to heads we have a second type of collision. The analysis of time series shows that the first type is more frequent.

The 1D model [38,67,49] can be an adequate model for the coin only in a particular case; (i) the coin mass center moves along one plane, (ii) the vector of the coin total angular velocity is perpendicular to the plane determined by its mass center trajectory.

The angle between the angular momentum and the normal to the coin is constant along the coin trajectory only when the air resistance is neglected so that the results of [13] which are based on this property cannot be always generalized.

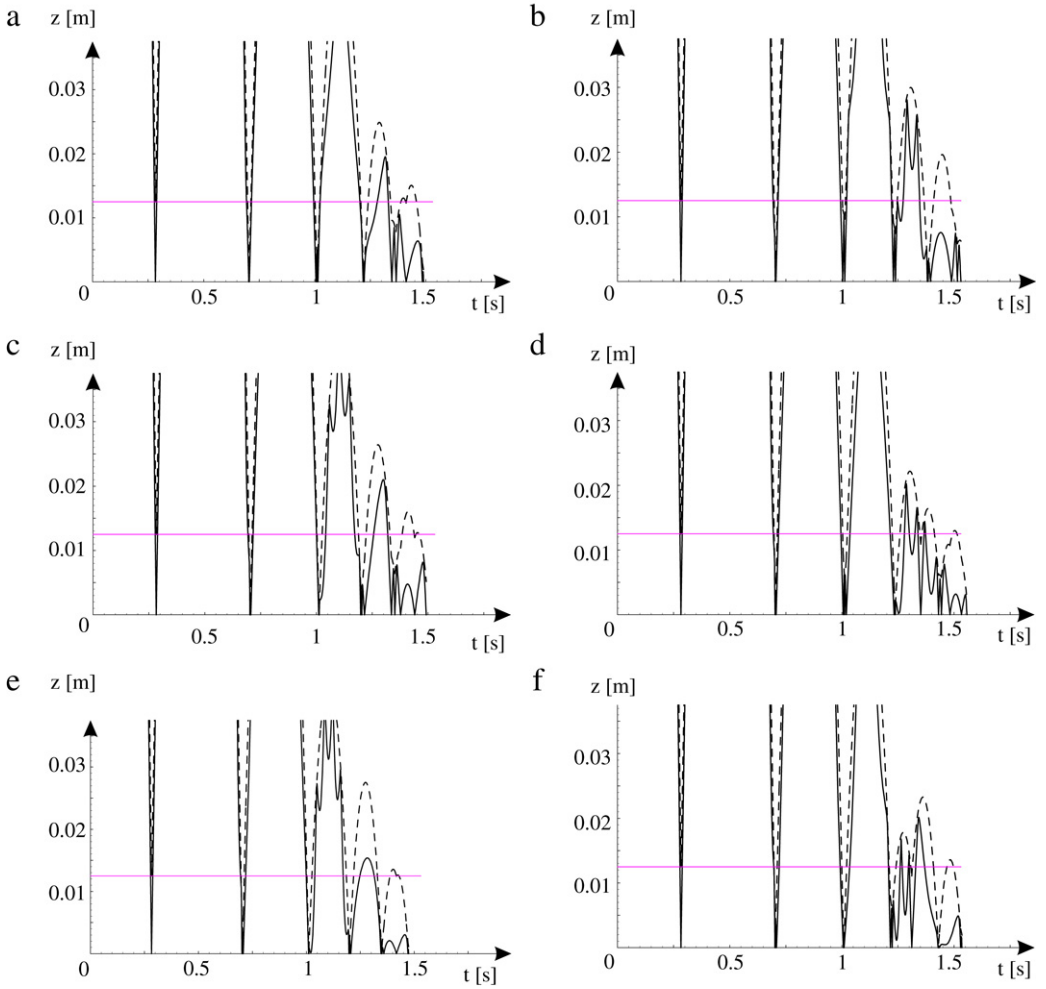

Fig. 24. Results of coin tossing: (a) $z_0 = 0.40001$, (b) $z_0 = 0.40002$, (c) $z_0 = 0.40003$, (d) $z_0 = 0.40004$, (e) $z_0 = 0.40005$, (f) $z_0 = 0.40006$ (in all cases: $\omega_{\eta 0} = 40.15$ rad/s, $x_0 = y_0 = 0$, $\dot{x_0} = \dot{y_0} = \dot{z_0} = 0$, $\varphi_0 = \psi_0 = 0$, $\vartheta_0 = 7\pi/180$ rad, $\omega_{\xi 0} = \omega_{\zeta 0} = 0$, $\omega_{\eta 0} = 40.15$ rad/s, $\lambda_n = 0.8$, $\lambda_\tau = 0.2$, $\chi = 0.8$).

Summarizing, we found that for the real coin, in which the distance between the center of the mass and the geometrical center is small, it is sufficient to consider a simplified model of the ideal thin coin. When the distance of the free fall is small, the effect of the air resistance is hardly visible and can be neglected.

5.2. *Why the dynamics is predictable?*

The equations of motion (29)–(39) given in Section 4 are Newton's equations, with no external source of random influence, i.e., the fluctuations of air, thermodynamic or quantum fluctuations of the coin. One can construct a mapping of the initial conditions to a final observed configuration (heads or tails). The initial conditions are: position, configuration, momentum, and angular momentum at the beginning of the free fall motion. There are three possible final configurations after bouncing on the floor: the coin terminates flat on the surface with it heads side up, its tails side up, or the coin balances on its edge. The first two configurations are stable. In some studies these are called stable point attractors [67,9], but the term attractor does not exactly coincide with the definition known in nonlinear dynamics. The flow given by the equations of motion maps all possible initial conditions into one of the final configurations. The set of initial conditions which are mapped onto heads configuration create *heads basin of attraction* while the set of initial conditions mapped onto tails configuration create *tails basin of attraction*. The boundary which separates heads and tails basins consists of initial conditions mapped onto the coin standing on the edge configuration. For an infinitely thin coin this set is a set of zero measure and thus with probability one the coin ends up either heads or tails. For the finite thinness of the coin this measure is not zero but the probability of edge configuration to be stable is low.

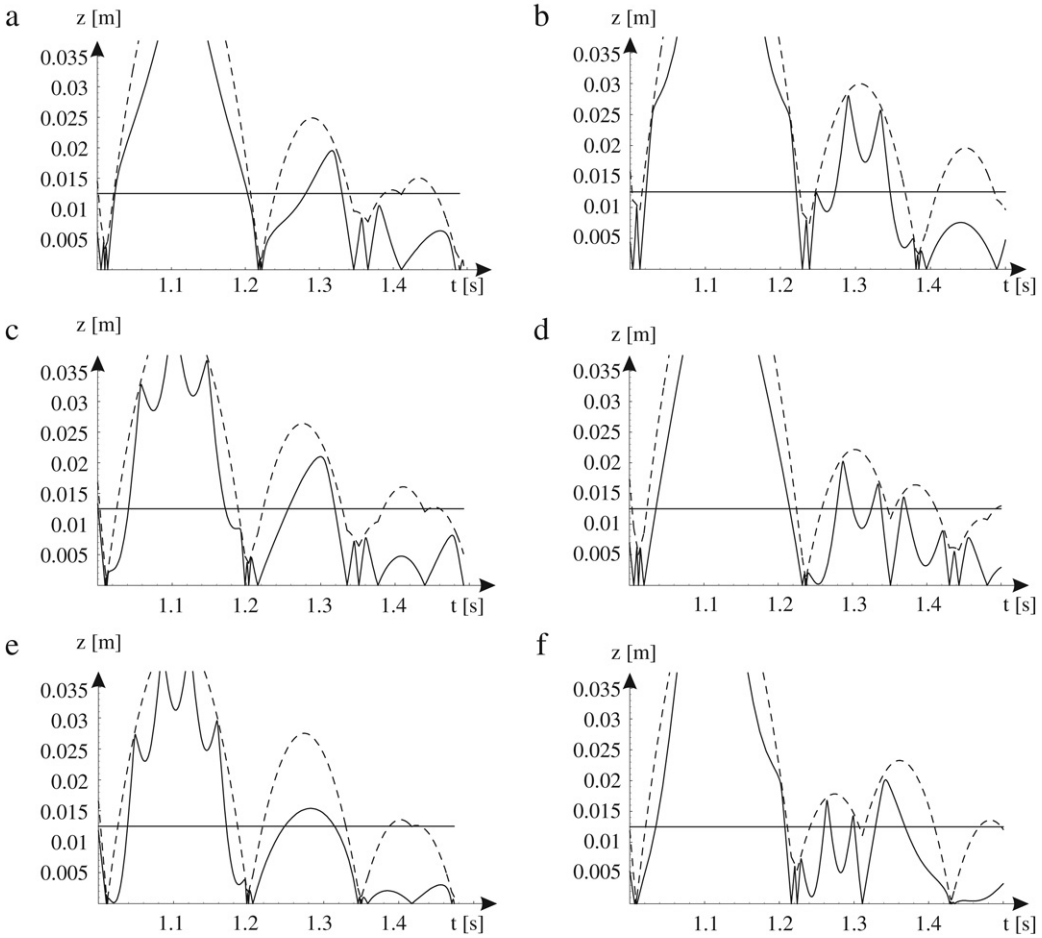

Fig. 25. Detailed view ($t \in (1,\ 1.5)$) of coin tossing results: (a) $z_0 = 0.40001$, (b) $z_0 = 0.40002$, (c) $z_0 = 0.40003$, (d) $z_0 = 0.40004$, (e) $z_0 = 0.40005$, (f) $z_0 = 0.40006$ (in all cases: $\omega_{\eta 0} = 40.15$ rad/s, $x_0 = y_0 = 0$, $\dot{x_0} = \dot{y_0} = \dot{z_0} = 0$, $\varphi_0 = \psi_0 = 0$, $\vartheta_0 = 7\pi/180$ rad, $\omega_{\xi 0} = \omega_{\zeta 0} = 0$, $\omega_{\eta 0} = 40.15$ rad/s, $\lambda_n = 0.8$, $\lambda_\tau = 0.2$, $\chi = 0.8$).

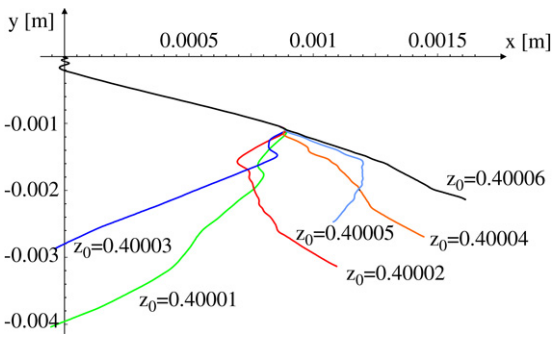

Fig. 26. Trajectories of the coin mass center: $z_0 = 0.40001$, $z_0 = 0.40002$, $z_0 = 0.40003$, $z_0 = 0.40004$, $z_0 = 0.40005$, $z_0 = 0.40006$ (in all cases: $\omega_{\eta 0} = 40.15$ rad/s, $x_0 = y_0 = 0$, $\dot{x_0} = \dot{y_0} = \dot{z_0} = 0$, $\varphi_0 = \psi_0 = 0$, $\vartheta_0 = 7\pi/180$ rad, $\omega_{\xi 0} = \omega_{\zeta 0} = 0$, $\omega_{\eta 0} = 40.15$ rad/s, $\lambda_n = 0.8$, $\lambda_\tau = 0.2$, $\chi = 0.8$).

If the outcome of the long sequence of the coin tossing is to give a random result, it can only be because the initial conditions vary sufficiently from toss to toss. Assume the one that can set the initial conditions $\Phi = \{x_0,\ y_0,\ z_0,\ \dot{x}_0,\ \dot{y}_0,\ \dot{z}_0,\ \psi,\ \vartheta,\ \varphi,\ \omega_{\xi 0},\ \omega_{\eta 0},\ \omega_{\zeta 0}\}$ with uncertainty ϵ. If the ball B in the phase space centered at Φ contains only points which go to one of the final states, the outcome is predictable and repeatable. If in the ball B there are points leading to different final states (denote the set of points leading to heads as H and the set points leading to tails as T), then the result of tossing is not predictable. One can calculate the probability of heads (tails) as prob(heads) $= \mu(H)/\mu(B)$ (prob(tails) $= \mu(T)/\mu(B)$) where μ is a measure of the sets H, T and B.

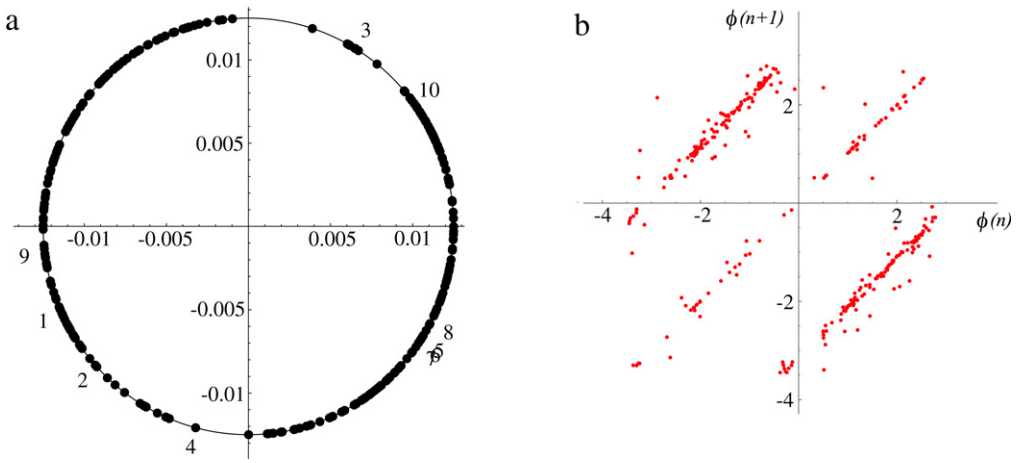

Fig. 27. Numerical simulation of the map S: (a) positions of collision point on the coin, (b) $\phi(n) - \phi(n+1)$ ($\vartheta = 25.021 \cdot \pi/180$, coefficient of restitution $\chi = 1$, air resistance considered, number of collisions 316).

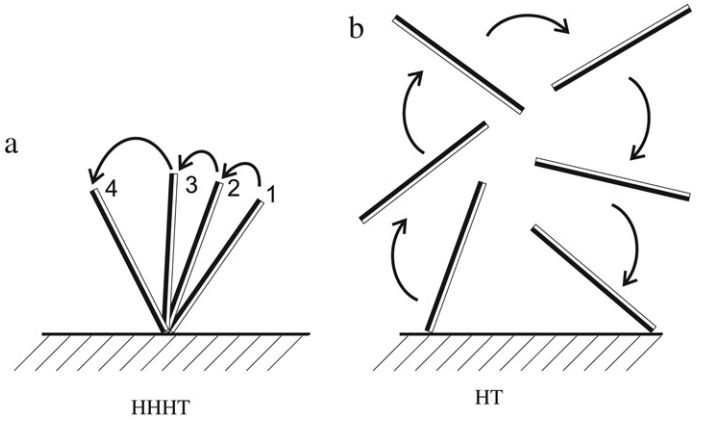

Fig. 28. Two types of collisions leading to the change of the coin face: (a) sequence of soft chattering collisions with small angular momentum transfer, (b) collision with large angular momentum transfer.

It is worth investigating the possibility that heads–tails basin boundaries are fractal [21], riddled [2,63,55,36] or intermingled [2,35]. Near a given basin boundary, if the initial conditions are given with the uncertainty ϵ, then a fraction $f(\epsilon)$ of initial conditions give an unpredictable outcome. In the limit $\epsilon \to 0, f(\epsilon) \sim \epsilon^{\alpha}$ where $\alpha < 1$ for fractal and $\alpha = 1$ for smooth boundary. Fractal basin boundaries are discontinuous (an uncountable sequence of disjoint stripes) or continuous (a snowflake structure) [45]. From the point of view of the predictability of the coin toss the possibility of the occurrence of intermingled basins is the most interesting. One can say that the outcome of the coin tossing procedure is not predictable if the basins of attraction of heads and tails are intermingled [2,35,55]. Let us briefly explain the term of intermingled basins of attraction. Let A be an attractor with a basin of attraction $\beta(A)$, which has a positive Lebesgue measure and contains a neighborhood of A. A basin $\beta(A)$ which has a positive Lebesgue measure but does not contain any neighborhood of the attractor A is called a riddled basin, i.e., for any point in the riddled basin of the attractor a ball in the phase space of arbitrarily small radius has a nonzero fraction of its volume in some other (say B) attractor basin. The basin of the attractor B may or may not be riddled by the basin $\beta(A)$. If the basin $\beta(B)$ is also riddled by the basin $\beta(A)$ we call such basins the intermingled ones. In the case of the tossed coin the intermingled basins of attraction between heads and tails will mean that in any neighborhood of the initial condition leading to heads there are initial conditions which are mapped to tails, i.e., there does not exist an open set of initial conditions which are mapped to one of the final states or infinitely small inaccuracy in the initial conditions makes the state of the coin tossing unpredictable.

As has already been mentioned in Section 1 basin boundaries for the simplest 1D model of the coin are given by the equidistant hyperbolas [38] (Fig. 2). Fig. 29(a–d) shows the basins of attraction of heads and tails calculated for various coin models. The dark regions correspond to heads and the white ones to tails. The case of the coin terminating on the soft floor (restitution coefficient $\chi = 0$) in which the air resistance has been neglected is shown in Fig. 29(a). The same case with the air resistance is presented in Fig. 29(b). The models which allow the bouncing of the coin on the floor surface ($\chi = 0.6$) are

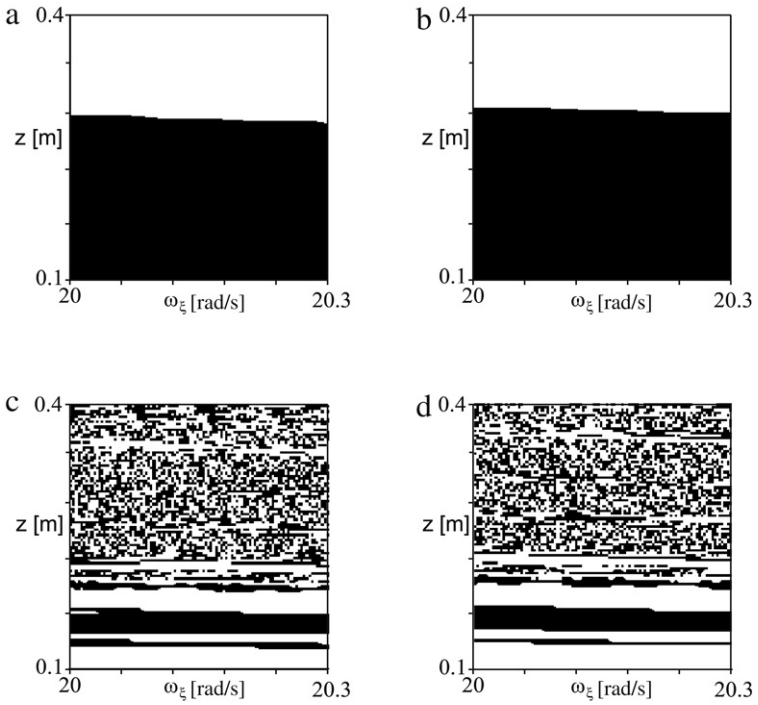

Fig. 29. Basins of attraction of heads (black) and tails (white), 2D model of an ideal thin coin described by Eqs. (37)–(39) has been simulated, (a, b) impactless motion, (c, d) motion with bouncing on the floor, (a, c) air resistance considered, $\lambda_n = 0.8$, $\lambda_\tau = 0.2$, (b, d) air resistance neglected.

shown in Fig. 29(c, d). In Fig. 29(c) and (d) the air resistance has been respectively neglected and considered. Fig. 29(a–d) has been calculated by numerically integrating Eqs. (37)–(39). We fixed all initial conditions except two namely: the position of the coin mass center z_0 and the angular velocity ω_ξ. We check that similar structures of the basin boundaries are observed when the different initial conditions are allowed to vary. So in Fig. 29(a–d) the 2D sections of the phase space are the good indications of what happens in the entire phase space.

The structure of the basin boundaries for the coin models without bouncing on the floor are similar to the boundaries in the Keller model [38]. It seems that the influence of the air resistance or the dimensionality of the model can be neglected (compare Fig. 2 with Fig. 29(a), (b)). One can notice that the structure of the basin boundaries is more complicated (looks like fractal or intermingled) when the coin is allowed to bounce on the floor as can be seen in Fig. 29(c, d). To check the possibility that these basins are fractal (intermingled) the appropriate enlargements are presented in Fig. 30(a–d). It can be seen that apart from the graininess due to the finite number of points, the boundaries are smooth (see Fig. 30(b, d)). Under further magnification no new structure can be resolved, i.e., no evidence of intermingled or even fractal basin boundaries is visible. The same conclusion has been reached in [67,49,37] where simple 1D models of the coin have been considered.

This allows us to state our main result: *for any initial condition Φ there exists such $\epsilon > 0$ that the ball with radius ϵ centered at Φ contains the points which belong either to set H or T*. In other words, if one can settle the initial condition with appropriate accuracy, the outcome of the coin tossing procedure is predictable and repeatable.

It should be mentioned here that based on the simple 1D models a similar conclusion has been reached in [67,49].

5.3. Why the tossed coin can approximate the random process?

If the outcome of the long sequence of coin tosses is to give random results, it can only be because the initial conditions vary from toss to toss. In the previous section we show numerically that for each initial condition there exists the accuracy $\epsilon > 0$ for which the final state is predictable. In this section we try to explain why for practically small (but not infinitely small) ϵ the coin tossing procedure can approximate the random process. A sequence of coin tosses will be random if the uncertainty ϵ is large in comparison to the width W of the stripes characterizing the basins of attraction so that the condition $\epsilon \gg W$ is essential for the outcome to be random [67]. It is interesting to notice that uncertainty ϵ depends on the mechanism of coin tossing while the quantity W is determined by the parameters of the coin.

As has been already shown in the previous subsection in the case of the coin bouncing on the floor the structure of the heads and tails basin boundary becomes complicated (Fig. 29(c, d)). In Fig. 30(a–d) we show the calculations of these basins for different number of impacts n. One observed the face of the coin which is up after the nth collision. Initial conditions leading to heads and tails are indicated respectively in black and white. The 2D model of an ideal thin coin described by Eqs.

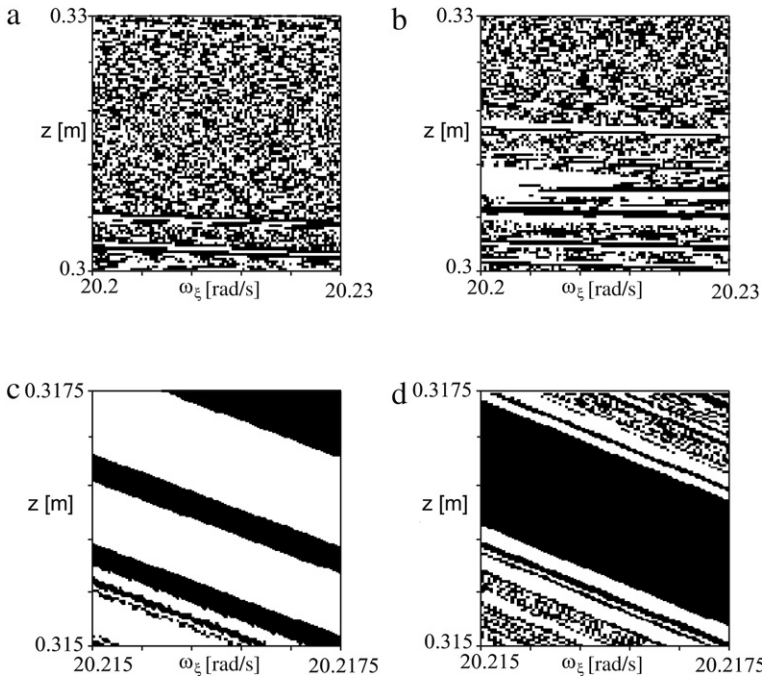

Fig. 30. Basins of attraction of heads (black) and tails (white), 2D model of an ideal thin coin described by Eqs. (37)–(39) has been simulated; (a, b) enlargements of Fig. 29(c), (c, d) enlargements of Fig. 29(d); (a, c) air resistance considered $\lambda_n = 0.8$, $\lambda_\tau = 0.2$, (b, d) air resistance neglected.

(37)–(39) has been simulated. In Fig. 30(a, c) the air resistance has been considered while in Fig. 30(b, d) air resistance has been neglected. Fig. 31(a, e), Fig. 31(b, f), Fig. 31(c, g) and Fig. 31(d, h) show results for respectively 0, 2, 5 and 9 collisions. With the increase of the collision numbers it is possible to observe that the complexity of the basin boundaries increases with the number of impacts. The increase of complexity is better visible when one considers the line in the phase space projection shown in Fig. 30(a–d) and count the number of crossings from one basin to another one N. It is possible to show that the function $N(n)$ grows faster than exponential. With the finite graininess (resolution) of Fig. 30(a–d) these basin boundaries look fractal and one can speak about fractalization like process which can be observed with the increase of impacts. Sensitivity to the initial conditions introduced during impacts (see Fig. 24) is responsible for this 'fractalization'. It seems that this mechanism is similar to the fractalization route to strange nonchaotic dynamics [12].

To explain this process consider the limit case of the infinite number of impacts which is possible in the unreal coin tossing model which neglects the air resistance and assumes the elastic impacts, i.e., $\chi = 1$. Consider the map $U : [0, 2\pi] \to [0, 2\pi]$ introduced in Section 5.1 shown in Fig. 32. Analysis of the time series of points $\phi_1, \phi_2, \ldots$, shows that the dynamics of U is chaotic as the largest Lyapunov exponent is positive (equal to 0.08). In this limit case the basins of heads and tails are intermingled and the outcome of the coin tossing is unpredictable. Numerically, this can observed when in the successive enlargements of the heads–tails basin boundaries the new structure is visible.

In the real case, the infinite number of impacts cannot be realized due to the dissipation (inelastic impacts and air resistance) so that the fractalization like process has to be stopped by the fulfillment of condition (20). The existence of the chaotic process described by the map U explains why the coins behave in practice as perfect randomizers.

6. Conclusions

In this review, we discuss the dynamics of the tossed coin under realistic circumstances. Using Euler parameters (normalized quaternions) we derive the equations of motion for the 3D imperfect coin which allows considering both the influence of the air resistance and the bouncing off the nonsmooth floor. We found that for the realistic coin in which the distance between the center of the mass and the geometrical center is small, it is sufficient to consider a simplified model of the ideal thin coin. The air resistance causes the deviation of the trajectory of the mass center from vertical axis and damps the rotation of the coin. When the distance of the free fall is small the effect of the air resistance can be neglected. During the free fall the sensitive dependence on the initial conditions has not been observed.

The process of the coin bouncing on the floor has a significant influence on the final state (heads or tails). It has been observed that the successive impacts introduce sensitive dependence on the initial conditions leading to transient chaotic behavior.

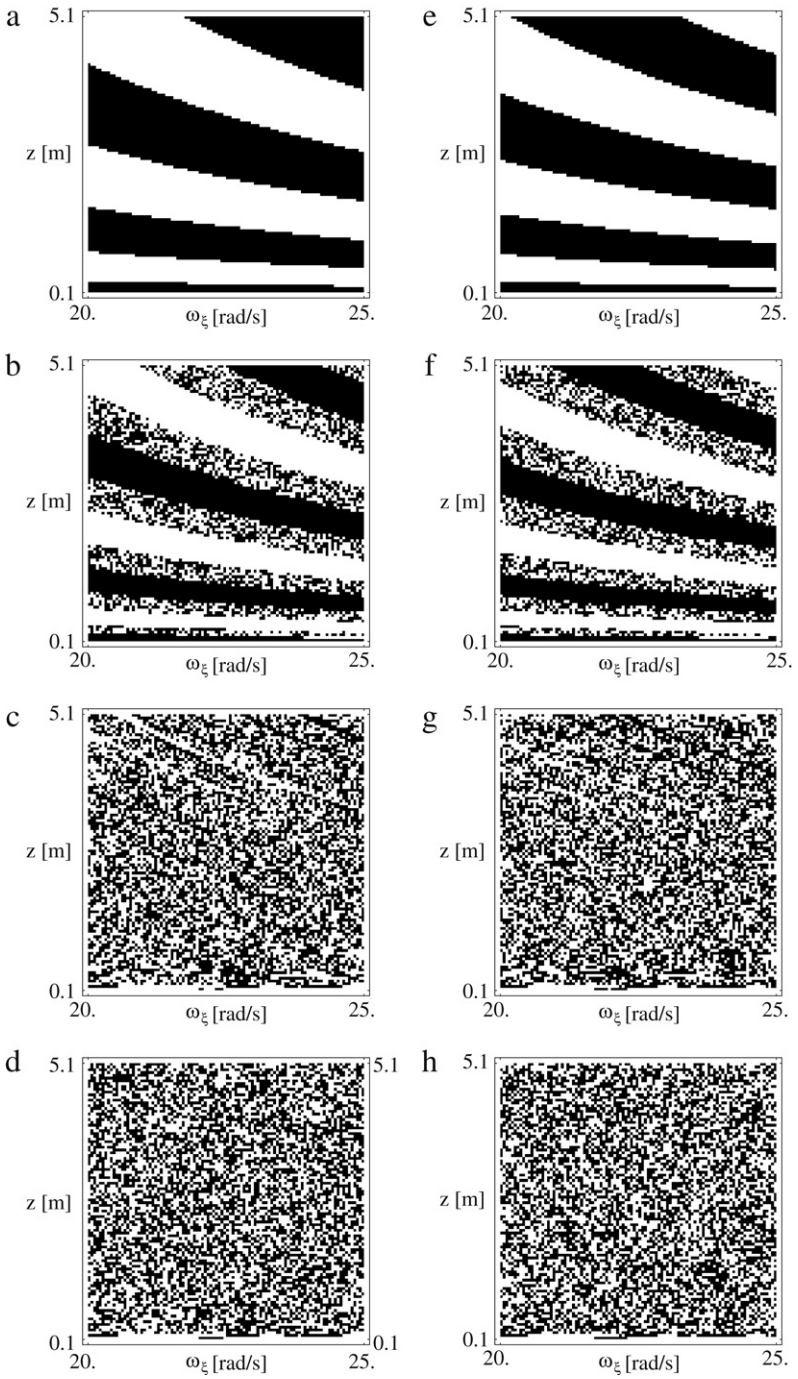

Fig. 31. Basins of attraction indicating the face of the coin which is up after the nth collision; 2D model of an ideal thin coin described by Eqs. (37)–(39) has been simulated, black and white indicate respectively basins of heads and tails; (a, e) $n = 0$, (b, f) $n = 2$, (c, g) $n = 5$, (d, h) $n = 9$; (a–d) air resistance considered, $\lambda_n = 0.8$, $\lambda_\tau = 0.2$, (e–h) air resistance neglected.

The basins of attraction of heads and tails (the sets of the initial conditions leading to both outcomes) show that the boundaries between heads and tails domains are smooth. This allow us to state our main result; there exists an open set of initial conditions for which the outcome of the coin tossing is predictable.

In practice although heads and tails boundaries are smooth the distance of a typical initial condition from a basin boundary is so small that practically any finite uncertainty in initial conditions can lead to the uncertainty of the result of tossing. This is especially visible in the case of the coin bouncing on the floor, when with the increase of the number

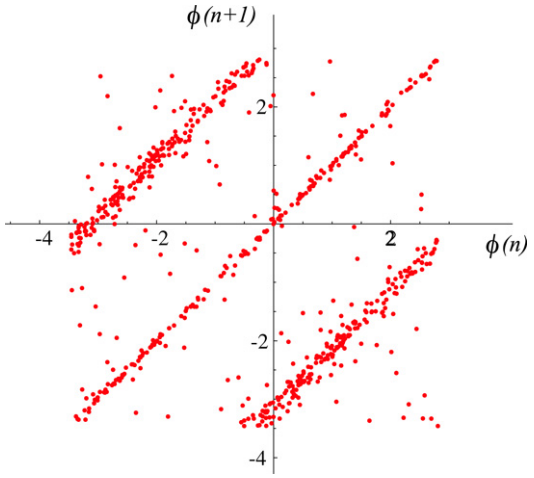

Fig. 32. Numerical simulation of the map S: (a) positions of collision point $\phi(n)$ on the coin, (b) $\phi(n) - \phi(n+1)$ ($\vartheta = 25.021 \cdot \pi/180$, coefficient of restitution $\chi = 1$, air resistance neglected, number of collisions is 700).

of impacts the basin boundaries become more complicated. In this case one can consider the tossing of a coin as an approximately random process.

Acknowledgment

This study has been partially supported by the Polish Department for Scientific Research (DBN) under project No. 4 T07A 044 28.

References

[1] The Holy Bible, American Standard Version of the Holy Bible, 1901.
[2] J.C. Alexander, J.A. Yorke, Z. You, I. Kan, Riddled basins, Internat. J. Bifurc. Chaos 2 (1992) 795.
[3] S.L. Altmann, Rotations, Quaternions, and Double Groups, Oxford University Press, Oxford, 1986.
[4] V.I. Arnold, Mathematical Methods of Classical Mechanics, Springer, New York, 1989.
[5] N.L. Balzass, R. Chatterjee, A.D. Jakson, Coin tossing as a billiard problem, Phys. Rev. E52 (1995) 3608.
[6] R. Barnhart, Beating the Wheel: Wining Strategies at Roulette, Lyle and Stuart, New York, 1992.
[7] T. Bass, The Eudaemonic Pie, Houghton-Mifflin, Boston, 1985.
[8] I. Benjamini, H. Kesten, Distinguishing sceneries by observing the scenery along a random walk, J. Anal. Math. 69 (1996) 97.
[9] N.P. Bhatia, G.P. Szego, Dynamical Systems: Stability Theory and Applications, Springer, New York, 1967.
[10] C. Cooper, Strange attractors in a chaotic coin flip simulation, Chaos Solitons Fractals 30 (2006) 1.
[11] C. Cooper, A note on on-off intermittency in a chaotic flip simulation, Comput. Graph. 31 (2007) 137.
[12] S. Datta, R. Ramakrishna, A. Prasad, Fractalization route to strange nonchaotic dynamics, Phys. Rev. 70 (2004) 046203.
[13] P. Diaconis, S. Holmes, R. Montgomery, Dynamical bias in the coin toss, SIAM Rev. 49 (2007) 211.
[14] J. Diebel, Representing attitude: Euler angles, unit quaternions, and rotation vectors. http://ai.stanford.edu/~diebel/, May 2007.
[15] Z. Duan, L. Howard, A modified gambler's ruin problem of polyethylene chains in the amorphous region, Proc. Natl. Acad. Sci. USA 93 (1996) 100007.
[16] E. Engel, A Road to Randomness in Physical Systems, Springer, New York, 1992.
[17] W. Feller, An Introduction to Probability: Theory and Examples, Wiley, New York, 1957.
[18] R.P. Feynman, R. Leighton, M. Sands, The Feynman Lectures on Physics, vol. 1, Addison-Wesley, New York, 1963.
[19] J. Ford, How random is a coin toss, Phys. Today 40 (1983) 3.
[20] H. Goldstein, Classical Mechanics, Addison-Wesley, Reading, 1950.
[21] C. Grebogi, S.W. McDonald, E. Ott, J.A. Yorke, Phys. Lett. 99A (1983) 415.
[22] H. Haken, Synergetic, Springer, Berlin, 1978.
[23] G. Harik, E. Cantu-Paz, D. Goldberg, B. Miller, The gambler's ruin problem, genetic algorithms, and the sizing of populations, Evol. Comp. 7 (1999) 231.
[24] M. Harris, M. Keane, Random coin tossing, Probab. Theory Related Fields 109 (1997) 27.
[25] E. Hopf, On causality, statistics and probability, J. Math. Phys. 13 (1934) 51.
[26] E. Hopf, Uber die Bedeutung der Willkurlinchen Funktionen fur die Wahrscheinlichkeitstheorie, Jahresbericht der DMV 46 (1936) 179.
[27] E. Hopf, Ein Verteilungsproblem bei dissipativen dynamischen Systemen, Math. Ann. 114 (1937) 161.
[28] D. Howard, Orthogonality of measures induced by random walks with scenery, Combin. Probab. Comput. 5 (1996) 247.
[29] H.M. Isomaki, J. von Boehm, R. Raty, Devil's attractors and chaos of a driven impact oscillator, Phys. Lett. 107A (1985) 343.
[30] H.M. Isomaki, J. von Boehm, R. Raty, Fractal basin boundaries of an impacting particle, Phys. Lett. 126A (1988) 484.
[31] Y. Itoh, H.A. Maechara, A variation to the ruin problem, Math. Japan 47 (1998) 97.
[32] E.T. Jaynes, Probability Theory: The Logic of Science, Cambridge University Press, Cambridge, 1996.
[33] T. Kapitaniak, Generating strange nonchaotic attractors, Phys. Rev. E 47 (1993) 1408.
[34] T. Kapitaniak, Distribution of transient Lyapunov exponents of quasi-periodically forced systems, Prorg. Theoret. Phys. 93 (1995) 831.
[35] T. Kapitaniak, Uncertainty in coupled systems: Locally intermingled basins of attraction, Phys. Rev. E 53 (1996) 53.
[36] T. Kapitaniak, Yu. Maistrenko, A. Stefanski, J. Brindley, Bifurcations from locally to globally riddled basins, Phys. Rev. E 57 (1998) R6253.
[37] Z. Kechen, Uniform distribution of initial states, Phys. Rev. A41 (1990) 1893.
[38] J.B. Keller, The probability of heads, Amer. Math. Monthly 93 (1986) 191.
[39] J.E. Kerrich, An Experimental Introduction to the Theory of Probability, J. Jorgensen, Copenhagen, 1946.
[40] A. Kmet, M. Petkovsek, Gambler's ruin problem in several dimensions, Adv. Appl. Math. 28 (2002) 107.

[41] L. Landau, E. Lifschitz, Mechanics, Pergamon Press, Oxford, 1976.
[42] L. Landau, E. Lifshitz, Fluid Mechanics, Butterworth and Heinemann, New York, 1987.
[43] T.F. Lindley, Is it the coin that is biased? Philosophy 56 (1981) 403.
[44] L. Long, H. Weiss, The velocity dependence of aerodynamic drag: A primer for mathematicians, Amer. Math. Monthly 106 (1999) 127.
[45] B.B. Mandelbrot, Fractal Geometry of Nature, Freeman, San Francisco, 1982.
[46] J.E. Marsden, T.S. Ratiu, Introduction to Mechanics and Symmetry, Springer, New York, 1994.
[47] B. McCormick, Aerodynamics, Aeronautics and Flight Mechanics, Wiley, London, 1995.
[48] Mathematica 4, Standard Add-on Packages, Wolfram Media, 1999.
[49] T. Mizuguchi, M. Suwashita, Dynamics of coin tossing, Progr. Theoret. Phys. Suppl. 161 (2006) 274.
[50] R. Mongomery, How much does a rigid body rotate? Amer. J. Phys. 59 (1991) 394.
[51] F. Mosteller, Fifty Challenging Problems in Probability with Solutions, Dover, New York, 1987.
[52] D.B. Murray, S.W. Teare, Probability of a tossed coin falling on its edge, Phys. Rev. E (1993) 2547.
[53] J.I. Nejmark, N.A. Fufajev, Dynamics of Nonholonomic Systems, in: Translations of Mathematical Monographs, vol. 33, American Mathematical Society, 1972.
[54] P.E. Nikrevesh, Computer-Aided Analysis of Mechanical Systems, Prentice-Hall, Englewood Cliffs, 1988.
[55] E. Ott, J.C. Alexander, I. Kan, J.C. Sommerer, J.A. Yorke, The transition to chaotic attractors with riddled basins, Physica D 76 (1994) 384.
[56] P. Pearle, Might God toss coin? Found. Phys. 12 (1982) 249.
[57] J. von Plato, Creating Modern Probability: Its Mathematics, Physics and Philosophy in Historical Perspective, Cambridge University Press, Cambridge, 1994.
[58] N. Platt, E.A. Spiegel, C. Tesser, On-off intermittency: A mechanism for bursting, Phys. Rev. Lett. 70 (1993) 279.
[59] H. Poincaré, Calcul de Probabilites, George Carre, Paris, 1896.
[60] A.L. Rocha, F. Stern, The asymmetric *n*-player gambler's ruin problem with equal initial fortunes, Adv. Appl. Math. 33 (2004) 512.
[61] E.J. Roth, Dynamics of a System of Rigid Bodies, Dover, New York, 1960.
[62] F. Scheck, Mechanics: From Newton's laws to deterministic chaos, Springer, Berlin, 1990.
[63] J.C. Sommerer, E. Ott, Riddled basins, Nature 365 (1993) 136.
[64] M. Stevens, Bigger than Chaos: Understanding Complexity thought Probability, Harvard University Press, Cambridge, 2003.
[65] T. Tel, Transient chaos, J. Phys. A 22 (1991) 691.
[66] P.A. Thompson, Compressible Fluid Dynamics, McGraw-Hill, London, 1972.
[67] V.Z. Vulović, R.E. Prange, Randomness of true coin toss, Phys. Rev. A33/1 (1986) 576.
[68] E.W. Weisstein, Coin Tossing. From MathWorld: A Wolfram Web Resource. http://mathworld.wolfram.com/CoinTossing.html.
[69] F.M. White, Viscous Fluid Flows, McGraw-Hill, London, 1991.
[70] E.T. Wittaker, Analytical Dynamics of Particles and Rigid Bodies, Cambridge University Press, Cambridge, 1937.
[71] Y. Zeng-Yuan, Z. Bin, On the sensitive dynamical system and the transition from the apparently deterministic process to the completely random process, Appl. Math. Mech. 6 (1985) 193.